

## A numerical study of tides in Titan's northern seas, Kraken and Ligeia Maria

Vincent, David; Karatekin, Özgür; Lambrechts, Jonathan; Lorenz, Ralph D.; Dehant, Véronique; Deleersnijder, Éric

**DOI**

[10.1016/j.icarus.2017.12.018](https://doi.org/10.1016/j.icarus.2017.12.018)

**Publication date**

2018

**Document Version**

Final published version

**Published in**

Icarus

**Citation (APA)**

Vincent, D., Karatekin, Ö., Lambrechts, J., Lorenz, R. D., Dehant, V., & Deleersnijder, É. (2018). A numerical study of tides in Titan's northern seas, Kraken and Ligeia Maria. *Icarus*, 310, 105-126. <https://doi.org/10.1016/j.icarus.2017.12.018>

**Important note**

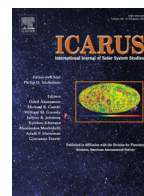
To cite this publication, please use the final published version (if applicable). Please check the document version above.

**Copyright**

Other than for strictly personal use, it is not permitted to download, forward or distribute the text or part of it, without the consent of the author(s) and/or copyright holder(s), unless the work is under an open content license such as Creative Commons.

**Takedown policy**

Please contact us and provide details if you believe this document breaches copyrights. We will remove access to the work immediately and investigate your claim.



# A numerical study of tides in Titan's northern seas, Kraken and Ligeia Maria

David Vincent<sup>a,\*</sup>, Özgür Karatekin<sup>b</sup>, Jonathan Lambrechts<sup>a</sup>, Ralph D. Lorenz<sup>c</sup>,  
Véronique Dehant<sup>b,d</sup>, Éric Deleersnijder<sup>e,f</sup>

<sup>a</sup>Institute of Mechanics, Materials and Civil Engineering (IMMC), Université catholique de Louvain, Avenue Georges Lemaître 4, B-1348 Louvain-la-Neuve, Belgium

<sup>b</sup>Royal Observatory of Belgium, Avenue Circulaire 3, B-1180 Bruxelles, Belgium

<sup>c</sup>Space Exploration Sector, Johns Hopkins Applied Physics Laboratory, Laurel, MD 20723, USA

<sup>d</sup>Earth and Life Institute (ELI), Université catholique de Louvain, Croix du Sud 2, B-1348 Louvain-la-Neuve, Belgium<sup>e</sup>

<sup>e</sup>Université catholique de Louvain, Institute of Mechanics, Materials and Civil Engineering (IMMC) & Earth and Life Institute (ELI), Avenue Georges Lemaître 4, B-1348 Louvain-la-Neuve, Belgium

<sup>f</sup>Delft Institute of Applied Mathematics (DIAM), Delft University of Technology, Mekelweg 4, 2628CD Delft, The Netherlands

## ARTICLE INFO

### Article history:

Received 13 July 2017

Revised 30 November 2017

Accepted 11 December 2017

Available online 12 December 2017

### Keywords:

Titan  
surface seas  
Tides  
liquid body  
Titan  
oceanography

## ABSTRACT

The tidal response of Titan's two largest northern seas, Ligeia Mare and Kraken Mare, is studied by means of a two-dimensional, depth-averaged, shallow water model, SLIM (<http://www.climate.be/slim>). Kraken Mare is formed of two basins, the northern one being assumed to be linked by a single strait, Trevize Fretum, to Ligeia Mare. The tidal motions tend to be independent of each other in each basin (i.e., Ligeia Mare, Kraken 1 and Kraken 2) which results in sharp transitions in the straits. Our results are overall rather similar to those of Tokano et al. (2014), suggesting that a 2D model such as SLIM is adequate for modelling Titan's tides and, since it is (presumably) less computationally demanding, may be better for sensitivity studies. For instance, the maximum tidal range in Kraken and Ligeia Maria respectively are 0.29 m and 0.14 m, which is within the range predicted by Lorenz et al. (2014) although smaller by 0.07 m and larger by 0.04 m than the estimates of Tokano et al. (2014) (but it occurs at the same location). The tidal currents are faster (by about one order of magnitude) in the straits linking those Maria than in the basins themselves (with a maximum of 0.36 m/s in the strait linking Kraken 1 and Kraken 2, Seldon Fretum). A decomposition of the tidal history into different harmonic components is carried out. Except in specific areas such as the straits and the amphidromic point(s), the main tidal component has a period of 1 Titan Day. We also briefly studied the eigenmodes of the northern seas whose period is close to the tidal period: such modes are very local. Indeed, their magnitude is significant (with respect to the magnitude of the modes elsewhere in the seas) in small bay(s) or near the islands of Kraken 2 and Ligeia Mare. They are not excited by the tides as they do not appear in the tidal motion.

A sensitivity analysis to poorly constrained parameters (bottom friction coefficient, depth of Trevize Fretum and attenuation factor – the latter is briefly discussed with respect to the values of the Love numbers found in the literature) is also conducted. The model parameters are seen to have a significant impact on the liquid exchanges between the basins and, consequently, on the tidal range and phase, fluid velocity and location of amphidromic point(s).

© 2017 Elsevier Inc. All rights reserved.

## 1. Introduction

Besides Earth, Titan is the only celestial body of the solar system on which liquid-filled surface lakes and seas have been detected. Liquid hydrocarbon lakes and seas have been assumed to be present on Titan's surface since *Voyager 1* established that the surface conditions of this icy moon were close to the triple point

of methane (Hanel et al., 1981; Samuelson et al., 1981). The Cassini spacecraft, which has been gazing at the Saturnian system since 2004, observed a methane cycle similar to the hydrological cycle on Earth (Atreya et al., 2006). It also detected possible surface lakes in Titan's southern hemisphere in 2004 (only some years later confirmed to be liquid) by means of its Imaging Science Sub-system (McEwen et al., 2005), and surface lakes and seas<sup>1</sup> in the

\* Corresponding author.

E-mail address: [david.vincent@uclouvain.be](mailto:david.vincent@uclouvain.be) (D. Vincent).

<sup>1</sup> The distinction between lake (Lacus) and sea (Mare) is based solely on the size.

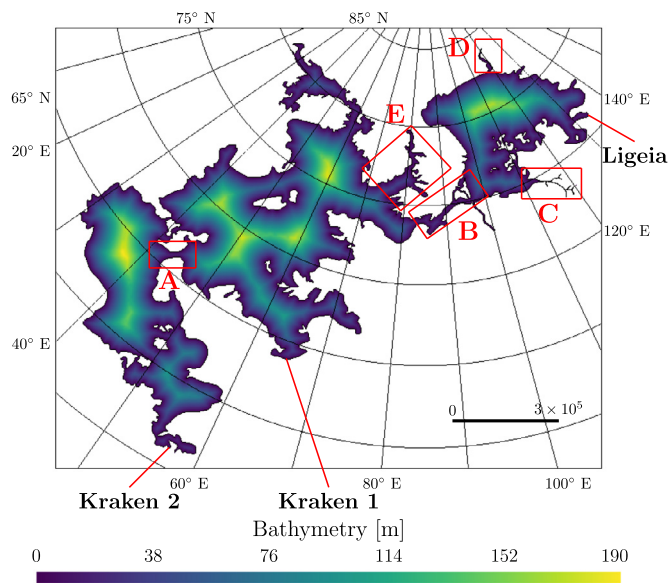


**Fig. 1.** Bathymetry map of Kraken and Ligeia Maria. The depth scales with the distance to the nearest shore, similarly to the bathymetry of Lorenz et al. (2014). The red letters refer respectively Seldon Fretum (A), Trevice Fretum (B), the canyons next to Vid flumina (C) and Xanthus Flumen (D), and Moray Sinus (E). (For interpretation of the references to color in this figure legend, the reader is referred to the web version of this article).

northern hemisphere in 2006 by means of its Radar (Stofan et al., 2007). The distribution of these surface lakes and seas is asymmetrical with respect to Titan's equator (Aharonson et al., 2009); there are many more lakes and seas in the northern hemisphere, where they are larger and deeper (Hayes et al., 2008). The surface lakes and seas are not the only liquid bodies of Titan: a global subsurface ocean has also been inferred from Cassini measurements (Iess et al., 2012). Stevenson (1992) was the first to suspect the presence of a global subsurface ocean beneath an icy shell. Since then, this assumption has been supported by several observations and measurements such as Titan's obliquity, its gravity field and its topography (Rappaport et al., 2008; Nimmo and Bills, 2010; Baland et al., 2011; 2014; Hemingway et al., 2013; Lefevre et al., 2014) and has been widely studied (e.g. Sohl et al., 1995; 2003; 2014; Beuthe, 2015). The global subsurface ocean results in significant deformations of the ice shell and, hence, of the lakes and seas bottom. Such deformations will reduce the tidal forcings to which surface liquids respond, since the ice crust itself partly follows the changing potential. This effect is modelled by an attenuation factor,  $\gamma_2$ , applied to the tidal forcing (Lorenz et al., 2014; Tokano et al., 2014; Beuthe, 2015). This factor depends on the internal structure of Titan and is particularly sensitive to the thickness, the rigidity and the rheological properties of the ice shell (e.g. Sohl et al., 2003; Lorenz et al., 2014; Tokano et al., 2014). As a consequence,  $\gamma_2$  should be considered as a free parameter (Lorenz et al., 2014).

In this study, we focus on two of the northern seas, Kraken Mare and Ligeia Mare. The former is the largest sea identified on Titan, with an area of at least 400,000 km<sup>2</sup>. It is centred at (68°N, 50°E) (Tokano, 2010) and it stretches from 55°N to 82°N (Lorenz et al., 2014). It is formed of two basins, Kraken 1 (in the north) and Kraken 2, linked by a strait named Seldon Fretum (identified by "A" in Fig. 1) and a set of small channels (Lorenz et al., 2014). It is about 17 km wide and 40 km long (Lorenz et al., 2014) which is similar to the dimensions of the Gibraltar strait on Earth. Ligeia Mare is located north-east of Kraken Mare: it is centred at (79°N, 112°E). Its maximal dimensions are about 420 by 350 km (Stofan et al., 2012). Recently, those seas have been found to be

linked by a strait, namely Trevice Fretum (identified by "B" in Fig. 1) (Sotin et al., 2012). The Cassini Radar altimeter also detected liquid filled canyons linked to Ligeia Mare in the northern and south-eastern regions of this sea (Poggiali et al., 2016) (identified by "C" and "D" in Fig. 1). Transient features called "Magic Islands" were observed in Kraken Mare and Ligeia Mare (Hofgartner et al., 2014; 2016). In Ligeia Mare, such phenomena were observed in regions centered at (78°N, 123°E) and (80°N, 111°E). They are best explained by ephemeral phenomena such as floating and/or suspended solids, bubbles, and waves while the diurnal phenomena, such as the tides, seem to be ruled out, the observations being all at nearly the same true anomaly (Hofgartner et al., 2016). In Kraken Mare, the phenomenon was observed at (73°N, 55°E). In this sea, the same explanations stand but the tides cannot be ruled out. We will study the tides induced by Saturn in the above-mentioned Maria and we will pay special attention to specific areas such as Seldon and Trevice Fretum, the aforementioned liquid filled canyons, and at the "Magic Islands" location.

Various studies were carried out about Titan's seas and lakes: bathymetry (e.g. Hayes et al., 2010; Ventura et al., 2012; Mastrogioseppe et al., 2014; Lorenz et al., 2014; Hayes, 2016), liquid composition (e.g. Brown et al., 2008; Cordier et al., 2009; Glein and Shock, 2013; Tan et al., 2013; 2015; Luspay-Kuti et al., 2015), dissipation due to friction in Titan's lakes and seas (e.g. Sagan and Dermott, 1982; Dermott and Sagan, 1995; Sears, 1995; Lorenz et al., 2014), tidal response (Tokano, 2010; Tokano et al., 2014; Vincent et al., 2016), interactions with the atmosphere (Tokano and Lorenz, 2015; 2016), and phenomena such as the shoreline variations of Ontario Lacus (Turtle et al., 2011) and the transient features in the northern seas Hofgartner et al. (2014; 2016). Among them, Tokano (2010); Lorenz et al. (2014); Tokano et al. (2014); Tokano and Lorenz (2015; 2016); Hofgartner et al. (2014; 2016) focused on the northern seas.

Tokano (2010) studied the tidal response of Kraken Mare using a 3D hydrostatic, baroclinic ocean circulation model based on a structured grid with a spatial resolution of 30 km. Due to the lack of information, he used a bathymetry scaling with the east-west distance from the closest shore (the maximum and minimum depth were respectively 500 m and 50 m) and the shoreline was not accurately represented (for instance, the connection with Ligeia Mare and the small channels near Seldon Fretum were ignored and Mayda Insula was considered to be an island). The impact of the ice shell deformations was not taken into account. According to his results, the tidal amplitude is minimum in the centre of the lake and increases with the distance to this point. He predicted a maximum tidal range (difference between high tide and low tide) of 4 m in the northern bay of Kraken 1 and he noticed that the tide rotates clockwise. The current is generally directed from places where the tide is low to places where the tide is high and its magnitude is maximum in Seldon Fretum (about 0.3 m/s) and offshore. Tokano (2010) took into account the seasonal effects through the solar heating: in winter, he predicted that the lake would be well mixed while it would be stratified in summer unless the evaporation cools down the lake surface. Lorenz et al. (2014) derived an analytical expression of the bathymetry and adapted Tokano (2010) results in order to take into account the surface deformations by multiplying the tidal amplitude by an attenuation factor  $\gamma_2$ . Tokano et al. (2014) improved the previous study of Tokano (2010): the bathymetry computed by Lorenz et al. (2014) was used, an attenuation factor  $\gamma_2 = 0.1$  was implemented to represent the impact of the ice shell deformations and the spatial resolution was 5.2 km. Ligeia Mare and Kraken Mare were linked and the small channels next to Seldon Fretum were considered as wide straits separated by islands (see Fig. 1 in Tokano et al. (2014)). The largest surface displacements predicted by the model were located in the south-eastern part

of Kraken 2 and northern part of Kraken 1 with a maximum tidal range of 0.37 m. The crucial role of the (unknown) depth of Seldon Fretum was pointed out by Lorenz et al. (2014) as well as Tokano et al. (2014). According to the latter, changing the depth of Seldon Fretum from 6 m to 100 m completely changes the character of Kraken Mare tides. For instance, it results in a phase lag of 90° and an increase of the maximum tidal range of 17 cm.

In this work, we will study the tidal response of Titan's northern seas by means of the state-of-the-art model SLIM, (<http://www.climat.be/slim>). It has already been used to predict the tidal response of a Titan lake, Ontario Lacus (see Vincent et al., 2016). SLIM solves the 2D depth-averaged shallow water equations on an unstructured grid (see Section 2.3), which allows an accurate representation of the shoreline and a higher resolution in the straits without the computational overhead of a regular but high resolution. We will also focus on the tidally induced liquid exchanges between the basins. Various parameters are poorly constrained, notably the roughness of the bottom and the depth of the straits linking the basins of the Maria. Their impact(s) and that of Titan's surface deformation will be quantified through a sensitivity analysis. We will also briefly study the impact of the bathymetry by implementing a bathymetry similar to that displayed in Fig. 9a of Hayes (2016) in Ligeia Mare and by varying the slope of the bottom in Kraken Mare. Finally, the impact of the shape of the shoreline on the tidal response will be studied by comparing our results with those obtained previously by means of other models. For the reference case, the bathymetry implemented scales with the distance to the shore (see Section 2.3) so that the maximum depth in Ligeia Mare is 170 m and the attenuation factor is set to  $\gamma_2 = 0.1$ , similarly to Tokano et al. (2014).

The goal of this study is to discuss the tidal response of Kraken and Ligeia Maria. This could also be helpful in enhancing our understanding of observed transient events and for planning future missions. Furthermore, being able to accurately predict the tidal response of the northern seas could allow assessing some parameters from future data. For instance, if we could measure accurately the sea surface elevation, we could infer the value of  $\gamma_2$ , which will give further insights into Titan's internal structure.

This article is organised as follows. Section 2 briefly describes the numerical model used, the forcings as well as the mesh and bathymetry implemented. In Section 3, the tidal response of the seas is studied, with a focus on the liquid exchanges between the basins, the volumetric flow rate through the main straits, the canyons of Ligeia Mare, Moray Sinus and the magic islands phenomenon. A sensitivity analysis to the attenuation factor, the depth of Trevice Fretum, the bathymetry scaling factor, the influence of the artificial bathymetry, and Manning's coefficient is conducted in Section 4. The results and the applications to and implications for future missions are respectively discussed in Sections 5 and 6. Conclusions are drawn in Section 7.

## 2. Method

The model is briefly introduced in Section 2.1 (for further details, see Vincent et al., 2016). The tidal forcing applied is described in Section 2.2 while the computational domain, the bathymetry and the mesh are described in Section 2.3. The value of the parameters of the models which are likely to have a significant impact on the results are discussed in Section 2.4.

### 2.1. Depth-averaged model

The numerical model used is the same as in Vincent et al. (2016): it is the Second-generation Louvain-la-Neuve Ice-ocean Model, SLIM. This model relies on the discontinuous Galerkin finite element method (DGFEM) to solve the

2D depth-averaged shallow water equations on an unstructured mesh. An implicit Runge–Kutta scheme using a Newton–Raphson solver is resorted to, which allows for time steps as large as five thousandths of a Titan day ( $\sim 6890$  s) to be used. This method does not suffer from excessive numerical dissipation or spurious oscillations. Furthermore, it is highly parallelisable, local mass conservation is ensured and an efficient wetting-drying algorithm to deal with the tidal flats is implemented (Kärnä et al., 2011). Solving the equations on unstructured grids is another advantage of this method. Indeed, the mesh can be refined at places of particular interest (for example, in the vicinity of the shores or in the straits) without significantly increasing the computational cost. SLIM has already been successfully used to simulate tides in various terrestrial domains including the Scheldt estuary (e.g., de Brye et al., 2010), the Mahakam delta (e.g., de Brye et al., 2011), and the whole Great Barrier Reef (e.g., Lambrechts et al., 2008). It has also been used on Titan in order to study Ontario Lacus (see Vincent et al., 2016).

Due to the absence of *in situ* measurements, models have to be used to determine the chemical composition and, hence, the density of Titan's lakes and seas. The dominant compounds can be determined from physical properties inferred from Cassini measurements such as the loss tangent and the dielectric permittivity (see e.g. Le Gall et al., 2016; Hayes, 2016) and different models were proposed (see e.g. Cordier et al., 2009; Glein and Shock, 2013; Tan et al., 2013; 2015; Luspay-Kuti et al., 2015). They all predicted that the seas and lakes are mainly composed of methane and ethane, other low-molecular-mass hydrocarbons, and nitrogen. Nevertheless, depending on the model or some parameters, the polar lakes and seas appear to be either ethane-rich or methane-rich, which modifies properties such as the liquid density and viscosity. Furthermore, the liquid composition varies with temperature (Glein and Shock, 2013). Consequently, the liquid composition can vary from one lake to another and over the year. For instance, according to Le Gall et al. (2016), Hayes et al. (2016), Ligeia Mare is methane rich and variation in backscattering between Ligeia Mare and Kraken Mare seems to suggest that Kraken Mare would have more ethane than Ligeia Mare, as assumed by Lorenz (2014). This could induce a density gradient in Trevice Fretum. Nevertheless, due to the sparse information about the composition of Kraken Mare, we do not take into account such density gradient in the present study. On the other hand, previous studies have shown that small variations of the mean density have a negligible impact on the tidal response (Vincent et al., 2016). Regarding to the temporal variations of the liquid composition, those induced by daily modifications of the surface temperature are negligible, diurnal variations disappearing at latitudes higher than 20°N (Cottini et al., 2012) while local variations induced by meteorological events are beyond the scope of this study, the associated time scale being much larger than that of the tides. Therefore, the density is assumed to be spatially and temporally constant in the northern seas. As the radar measurements (Hayes et al., 2016) and the independent microwave radiometry data (Le Gall et al., 2016) indicate quite clearly that methane dominates the composition (at least of Ligeia Mare), the density is set to 550 kg/m<sup>3</sup> in agreement with Tan et al. (2015).

Several assumptions are made in order to derive the governing equations solved hereinafter from the general mass and momentum conservation equations. First, density variations are disregarded, as aforementioned. Second, the maximum depth is about 189 m, which is much smaller than the horizontal length scale. Such a small aspect ratio is also observed in Seldon and Trevice Fretum. The aspect ratio being small, the hydrostatic approximation holds valid. Third, we neglect the atmospheric pressure gradient as we focus on tidal motion. These assumptions allow for an

integration over the depth resulting in the 2D equations solved by our model (see Eq. 1 of Vincent et al., 2016).

Eddy viscosity and bottom friction in the shallow water equations are parametrised by means of Smagorinsky's closure model (Smagorinsky, 1963) and an empirical Earth-based formula, the Chézy-Manning-Strickler's formulation (see, e.g., Lambrechts et al., 2008). Accordingly, the bottom stress is estimated as follows:

$$\tau_b = \rho g n^2 \frac{|\mathbf{u}| \mathbf{u}}{H^{1/3}}$$

where  $\rho$  is the density;  $g = 1.352 \text{ m/s}^2$  is the mean gravitational acceleration;  $\mathbf{u}$  is the depth-averaged velocity;  $H = h + \eta$  is the total liquid depth of the lake where  $h$  is the reference height of the water column and  $\eta$  is the sea surface elevation (positive upward); and  $n = 0.03 \text{ sm}^{-1/3}$  is Manning's roughness coefficient (it corresponds to natural river bottom on Earth).

The interactions with the atmosphere are neglected: we take into account neither the precipitations, nor the evaporation, nor the wind stress.

## 2.2. Astronomical forcings

The forcings taken into account are those induced by Saturn while those due to other moons and the Sun are neglected. Indeed, the latter is one order of magnitude smaller while the other moons are much smaller than Saturn, resulting in a smaller attraction potential. The ocean tidal loading due to the adjacent sea(s) is neglected as suggested by Tokano et al. (2014). The tidal forcing is obtained from the horizontal gradient of the tidal potential. As Titan is a tidally locked moon, the two main contributions to the astronomical forcing are that due to the orbital eccentricity (derived by Dermott and Sagan, 1995) and that due to Titan's obliquity (derived by Tyler, 2008), whose period is 1 Titan day (*TD*).

The ideal tidal forcing due to the horizontal gradient of the tidal potential would be completely effective on a totally rigid moon. Nevertheless, Titan is not rigid, it is even highly deformable compared to the Earth: the deformations of the ice shell above the global subsurface ocean are much larger than the deformations of the Earth crust. The solid tides of Titan and the resulting sea bottom displacements are thus much more significant. The influence of such solid tides on the tidal potential can be modelled through the attenuation factor  $\gamma_2 = 1 + \Re(k_2) - \Re(h_2)$  where  $\Re(k_2)$  and  $\Re(h_2)$  respectively are the real part of the second degree tidal potential Love number and the second degree radial displacement Love number (Sears, 1995; Sohl et al., 1995; Lorenz et al., 2014; Tokano et al., 2014; Beuthe, 2015). This attenuation factor represents the fact that Titan surface deformations will reduce the tidal forcing to which surface liquids respond. It is consequently implemented as a factor multiplying the tidal forcing in the shallow water equations: the term representing the tidal forcing is  $\gamma_2 \nabla_h \phi$  where  $\nabla_h$  is the horizontal del operator and  $\phi$  is the tidal potential. Love numbers  $k_2$  and  $h_2$  respectively characterize the ratio of the potential due to the ice shell deformations to the tidal potential and the ratio of the solid tide height to the height of an equilibrium ocean. Such a factor is also used to model solid Earth and ocean tides (e.g. Hendershott, 1972; Gordeev et al., 1977). Nevertheless, there are uncertainties about these Love numbers: they depend on the subsurface ocean thickness and density, on Titan's internal structure, on the rheological properties of Titan (Sohl et al., 2003), on the ice shell rigidity (Lorenz et al., 2014; Rappaport et al., 2008), and they vary linearly with the ice shell thickness (Sohl et al., 2003; Rappaport et al., 2008). Consequently, we decided to consider  $\gamma_2$  as a free parameter (as recommended by Lorenz et al., 2014). The range of acceptable values of parameter  $\gamma_2$  is briefly discussed in Section 2.4. For the reference case, we chose  $\gamma_2 = 0.1$  to match with Tokano et al. (2014).

## 2.3. Computational domain and bathymetry

We consider Ligeia and Kraken Maria independent from the other seas and lakes and without external fluid input due to hypothetical river(s). The shoreline contour is drawn from the Radar mosaic shown in Lorenz et al. (2014). The resolution of these images vary depending on the location: from 1 to 2 km in Kraken Mare and from 0.3 to 1 km in Ligeia Mare (Lorenz et al., 2014). Particular attention is paid to Seldon and Trevice Fretum (respectively point A and B in Fig. 1). The latter is elongated (200 km, five times longer than Seldon Fretum) and narrow (about 15 km, 2 km less than Seldon Fretum). As recently discovered, there are liquid filled canyons in Vid Flumina (Point C in Fig. 1) and Xanthus Flumen (Point D in Fig. 1), near Ligeia Mare (Poggiali et al., 2016). Nevertheless, as they do not impact the tides in the northern seas, they are not included in our domain except for studying the tidal motion therein (see Section 3.3). At Vid Flumina location, the width of the implemented canyons is less than 1300 m, which is slightly larger than the observation of Poggiali et al. (2016) (they predicted a maximum width of 1000 m). Nonetheless, this value is only reached locally, at intersection, most of the canyons being narrower than 1000 m and the mean width is close to the value predicted by Poggiali et al. (2016) (700 m). Near Xanthus Flumen, there is a strait and a small widening before the start of the canyon. The canyon maximum width is about 6700 m (at the mouth of the canyon), which matches with the observations of Poggiali et al. (2016).

The unstructured meshes are generated by means of GMSH (see Geuzaine and Remacle (2009)), which is one of the most widely used open source unstructured mesh generator. The spatial resolution in the seas ranges from 1 km to 12 km. We use three refinement criteria:

- The local element size is proportional to the celerity of the long surface gravity waves,  $c = \sqrt{gh}$ , as suggested by Henry and Walters (1993), Legrand et al. (2006).
- The mesh is refined near the shores.
- The spatial resolution is increased in Trevice Fretum and Seldon Fretum (the minimum grid size is still 1 km but the maximum grid size is 3 km in these areas).

A bathymetry profile along the T91 flyby (in Ligeia Mare) was derived from Cassini measurements by Mastrogiuseppe et al. (2014) and a bathymetry map of Ligeia Mare is displayed in Fig. 9a of Hayes (2016). Nevertheless, due to the opacity of Kraken Mare to the radar waves no bathymetry profile is available except in Moray Sinus. Consequently, no measured bathymetry is available for Kraken Mare. Lorenz et al. (2014) derived a hypothetical bathymetry with a simple bottom shape: a constant slope was assumed away from the shore. Nevertheless, due to variations in the shoreline contour, we could not use this bathymetry. Consequently, we build our own bathymetry similarly to the method used by Lorenz et al. (2014) (see Fig. 2 in Tokano et al., 2014): the depth scales with the distance to the nearest shore (i.e.,  $depth = \alpha \times distance$ ), the scaling factor,  $\alpha$ , being computed in such a way that the maximum depth in Ligeia Mare is the same as in Lorenz et al. (2014) (i.e. 170 m) (see Fig. 1). It results in small local variations of the bathymetry due to small modifications of the shoreline or the fact that an island is taken into account or ignored. For instance, the maximum depth of the implemented bathymetry is 189 m and is located in Kraken 2 instead of Kraken 1 according to the bathymetry of Lorenz et al. (2014). We will briefly discuss to what extent an artificial bathymetry is justifiable in Section 4.4 by comparing our results with those obtained for a bathymetry of Ligeia Mare that mimics Fig. 9a of Hayes (2016).

## 2.4. Model parameters

Several parameters are likely to have a significant impact on the model results. A sensitivity analysis will be conducted with respect to four of them: the attenuation factor  $\gamma_2$ , the bathymetry of Kraken Mare, the depth of Trevice Fretum  $H$ , and Manning's roughness coefficient  $n$ . The latter is studied within a range from 0.01 to  $0.06 \text{ sm}^{-1/3}$ , which respectively corresponds to smooth man-made channel and to natural channels with stones on Earth. The results are presented in Section 4.3.

As explained in Section 2.3, the bathymetry is not derived from measurements but is assumed to scale with the distance to the shore, the scaling factor,  $\alpha$ , being set to reach the same maximum depth in Ligeia Mare as in the bathymetry map of Lorenz et al. (2014). However, there is no evidence to suggest that the scaling factor is the same in Kraken Mare. Consequently, we consider two additional cases: in case 1, we multiplied the scaling factor by 2 (i.e.,  $\text{depth} = 2\alpha \times \text{distance}$ ) and, in case 2, we divided it by 2 (i.e.,  $\text{depth} = 0.5\alpha \times \text{distance}$ ). The former and latter case are referred to as *bathy A* and *bathy B*. For *bathy B*, the maximum depth is 170 m and lies in Ligeia Mare; the maximum depth in Kraken 1 and Kraken 2 respectively are 92 m and 95 m. For *bathy A*, the maximum depth in Kraken 1 and Kraken 2 respectively are 365 m and 379 m. It results in significant modifications of the volume ratio between Kraken and Ligeia Mare. The variations of the tidal response induced by such modifications are detailed in Section 4.5. Furthermore, as pointed out by Tokano et al. (2014), the depth of Seldon Fretum (which is underconstrained) has a significant impact on the tidal current inside the strait. It is likely that the depth of Trevice Fretum, which is also not well constrained, has a similar impact. Consequently, we consider the depth of this strait as a free parameter. We carried out simulations for four cases: the reference case and three constant depths. For the reference case, the depth increases with the distance to the shore, which results in a maximum depth of 15 m and a bottom profile which has the shape of a “v”. The three other cases correspond to a bottom profile which has the shape of a “L” and whose depths respectively are 10 m, 20 m, and 50 m. The impact of this parameter is detailed in Section 4.2.

The attenuation factor value is a function of the Love numbers  $k_2$  and  $h_2$  which, in turn, depends on the internal structure of Titan. Unfortunately, the latter is poorly constrained, which results in uncertainties about these Love numbers. less et al. (2012) derived some values of  $k_2$  from Cassini measurements by means of three analysis models while Sohl et al. (2003), Sohl et al. (2014), Baland et al. (2014), Lefevre et al. (2014), Beuthe (2015), among others, used models to reconstruct Titan's internal structure from observations and measurements such as the gravity field, the second degree tidal potential Love number  $k_2$  and the moment of inertia (which was recently questioned by Hemingway et al. (2013), Baland et al. (2014) and Lefevre et al. (2014)). As a result, different values can be found depending on the working hypotheses and the model used (see Table 1).

Beuthe (2015) predicted values of  $k_2$  matching with those computed by less et al. (2012) from observations. By setting the ice shell relative thickness in order to correspond with the value of  $k_2$  obtained by less et al. (2012), the corresponding attenuation factors range from 0 to 0.21 depending on the density of the crust and subsurface ocean (See Fig. 5 in Beuthe, 2015). Tokano et al. (2014) computed  $\gamma_2$  for different internal structures and only retained those which satisfy the moment of inertia and the Love number  $k_2$  predicted by less et al. (2012), which results in  $\gamma_2 \in [0.1, 0.2]$  depending on the ice shell thickness. However, the value retained from the moment of inertia was obtained by having recourse to the hydrostatic assumption, which is questionable due to the significant degree-three signal observed in the gravity

field (Hemingway et al., 2013; Lefevre et al., 2014; Baland et al., 2014). All these models assume a thin and homogeneous crust. However, the crust could be non-homogeneous: there could be some clathrates outgassing methane in the atmosphere from time to time (Tobie et al., 2006). Such clathrates at the base of the ice shell might have a smaller shear modulus which would cause larger deformations of the shell and the Love number  $k_2$  would be larger (Rappaport et al., 2008).

In the light of the values found in the literature, we decided to study the tidal response for three additional values of  $\gamma_2$ : 0.05, 0.2, and 0.3 (see Section 4.1).

## 3. Results

In this section, we first describe the tidal response of Ligeia and Kraken Maria predicted by our model. For this purpose, we study the decomposition in different harmonic components as well as some of the northern seas eigenmodes. Then, we focus on some specific areas such as Trevice and Seldon Fretum, the canyons observed by Poggiali et al. (2016), Moray Sinus and the Magic islands locations. The bathymetry is that shown in Fig. 1, the attenuation factor is  $\gamma_2 = 0.1$  and Manning's coefficient is set to  $0.03 \text{ sm}^{-1/3}$ .

### 3.1. Tidal response of Kraken and Ligeia Maria

The tidal forcing (see Section 2.2) applied rotates anticlockwise with an exact period of  $1 TD$  (not shown). It is not unidirectional over the seas. Indeed, there can be a significant difference in forcing orientation between Ligeia Mare and Kraken Mare or even between the southern and northern region of Kraken Mare. For instance,  $0.25 TD$  after perikron/apokron (point of the orbit where Titan is nearest/farthest to Saturn), the angle between the direction of the forcing in the north-eastern and south-western regions can be larger than  $90^\circ$ . The forcing in  $t^*$  and  $t^* + T/2$  has the same magnitude but it is oriented in opposite directions. In Ligeia Mare, the maximum is about  $3.59 \times 10^{-7} \text{ m/s}^2$  and occurs  $0.1 TD$  before perikron/apokron in the eastern part of the sea while, in Kraken Mare, it is about  $5.46 \times 10^{-7} \text{ m/s}^2$  and it occurs  $0.145 TD$  after perikron/apokron in the south-eastern part of the southern basin.

The maximum/minimum sea surface elevation ( $\eta$ ) is  $\pm 0.145 \text{ m}$ . It occurs  $0.31 TD$  after perikron/apokron in the south-eastern part of Kraken 2,  $0.165 TD$  after the maximum forcing magnitude which is directed south-westward (see the video in the additional content, available at [NorthernSeas\\_sse\\_reference\\_case.mp4](#)). The maximum/minimum sea surface elevation in Kraken 1 is  $\pm 0.115 \text{ m}$  and occurs  $0.18 TD$  before perikron/apokron at the north-western end of the basin. In Ligeia Mare, the maximum/minimum is  $\pm 0.07 \text{ m}$  and occurs  $0.05 TD$  before perikron/apokron at the eastern shore of Ligeia Mare. The sea surface elevation in Kraken 2 and Ligeia Mare can be positive/negative over the whole basin, which suggests strong liquid exchanges through the straits (see Section 3.2). It lasts longer in Ligeia Mare (about  $0.2 TD$ ) than in Kraken 2 (where the sea surface elevation is positive/negative over the whole basin during respectively  $0.095 TD$  and  $0.06 TD$ ) and does not occur in Kraken 1 due to the presence of the amphidromic point. The period of time during which the elevation is positive over the whole basin is not the same as that during which it is negative which suggests that the volumetric flow rate going through Seldon and Trevice Fretum is not the same at  $t^*$  than at  $t^* + T/2$ . The fact that the tidal motion is independent in each basin results in strong sea surface elevation gradient in the straits. This gradient is larger in the small channels near Seldon Fretum (the maximum is about  $2.22 \times 10^{-5}$ ) than in Seldon and Trevice Fretum where it can respectively reach about  $1 \times 10^{-5}$  and  $7 \times 10^{-6}$ . The gradient in-

**Table 1**

Real part of the Love numbers ( $\Re(k_2)$  and  $\Re(h_2)$ ) and attenuation factor ( $\gamma_2$ ) corresponding to the presence of a subsurface ocean (as established by Sohl et al. (2003), Sohl et al. (2014), Baland et al. (2014), Lefevre et al. (2014), Beuthe (2015) from observations and measurements) found in the literature.  $k_2$  and  $h_2$  respectively are the second degree tidal potential Love number and the second degree radial displacement Love number.

| Authors                         | $\Re(k_2)$        | $\Re(h_2)$   | $\gamma_2$   |
|---------------------------------|-------------------|--------------|--------------|
| Sohl et al. (1995)              | 0.36              | 1.19         | 0.17         |
| Sohl et al. (2003) <sup>a</sup> | [0.39, 0.32]      | [1.25, 1.05] | [0.13, 0.27] |
|                                 | [0.39, 0.35]      | [1.28, 1.15] | [0.12, 0.2]  |
| Nimmo and Bills (2010)          | –                 | 1.28         | –            |
| Iess et al. (2012) <sup>b</sup> | $0.589 \pm 0.075$ | –            | –            |
|                                 | $0.67 \pm 0.09$   | –            | –            |
|                                 | $0.637 \pm 0.112$ | –            | –            |
| Sohl et al. (2014)              | 0.437             | 1.29         | 0.147        |
| Beuthe (2015) <sup>c</sup>      | 0.7 – 0.5         | 1.7 – 1.3    | 0 – 0.2      |
|                                 | 0.7 – 0.41        | 1.7 – 1.2    | 0 – 0.21     |

<sup>a</sup> Various ice thickness and two ammonia concentrations.

<sup>b</sup> Different analysis models.

<sup>c</sup> Two crust densities and various relative thickness of the ice shell.

**Table 2**

Maximum amplitude<sup>2</sup> of the first tidal component and relation between the amplitude of the other tidal components and that of the first tidal component. In the basins, these values are computed at three points: (80°N, 110°E) in Ligeia Mare, (70°N, 50°E) in Kraken 1, and (62.5°N, 40°E) in Kraken 2. In the straits, they are computed where the relation  $\frac{\text{comp}2}{\text{comp}1}$  is maximum.

|                     | Period [TD] | Ligeia Mare <sup>b</sup> | Kraken 1 <sup>c</sup> | Kraken 2 <sup>d</sup> | Seldon Fretum | Trevize Fretum | Small channels |
|---------------------|-------------|--------------------------|-----------------------|-----------------------|---------------|----------------|----------------|
| Comp 1              | 1           | 0.027 m                  | 0.023 m               | 0.056 m               | 0.018 m       | 0.008 m        | 0.001 m        |
| Comp 2 <sup>a</sup> | 0.5         | 1%                       | 1%                    | 1%                    | 96%           | 62%            | 378%           |
| Comp 3 <sup>a</sup> | 1/3         | 2%                       | 4%                    | 3%                    | 3%            | 18%            | 58%            |
| Comp 4 <sup>a</sup> | 0.25        | 0%                       | 0%                    | 0%                    | 21%           | 10%            | 118%           |
| Comp 5 <sup>a</sup> | 0.2         | 0%                       | 1%                    | 1%                    | 1%            | 1%             | 48%            |
| Comp 6 <sup>a</sup> | 1/6         | 0%                       | 0%                    | 0%                    | 4%            | 1%             | 54%            |
| Comp 7 <sup>a</sup> | 1/7         | 0%                       | 0%                    | 0%                    | 1%            | 1%             | 34%            |

<sup>a</sup> Amplitude of the tidal component expressed as a percentage of the amplitude of the first tidal component.

<sup>b</sup> at (80°N, 110°E).

<sup>c</sup> at (70°N, 50°E).

<sup>d</sup> at (62.5°N, 40°E).

creases and decreases twice on a tidal cycle and can be very small during some short periods of time (see, for example, the sea surface elevation in the video in the additional content).

While studying the sea surface elevation of seas, it is common to study the tidal components. Indeed, the sea surface elevation at a point can be viewed as a sum of several components written as  $\eta(t, x, y) = E(x, y) \cos(\omega t + \phi(x, y))$  where  $E(x, y)$  is the amplitude<sup>2</sup>,  $\omega = 2\pi/T$  is the angular period, and  $\phi(x, y)$  is the tidal phase. On Titan, the first, second, third, and fourth tidal components respectively have a period of 1, 0.5, 0.33, and 0.25 TD. Fourier analysis shows that the first tidal component (whose period is 1 TD) is responsible for more than 90% of the sea surface motion, except for some small areas in the straits and at the amphidromic point of the first tidal component (see Fig. 2). The second and fourth components are significant in the straits (see Table 2) but can be neglected elsewhere while the third component is significant in Trevize Fretum and where the tidal range due to the first tidal component is weak (i.e. near the amphidromic point and in the south-western part of Kraken 2 (see Fig. 2)). The other tidal components are insignificant in comparison to the aforementioned components. In the small straits near Seldon Fretum, the tidal range of the second and fourth tidal components are larger than that of the first one. Nevertheless, it remains small (at most 0.017 m for the second). The fact that the amplitude of the others components is significant with respect to the first one in these straits is due to the small amplitude of the latter at this loca-

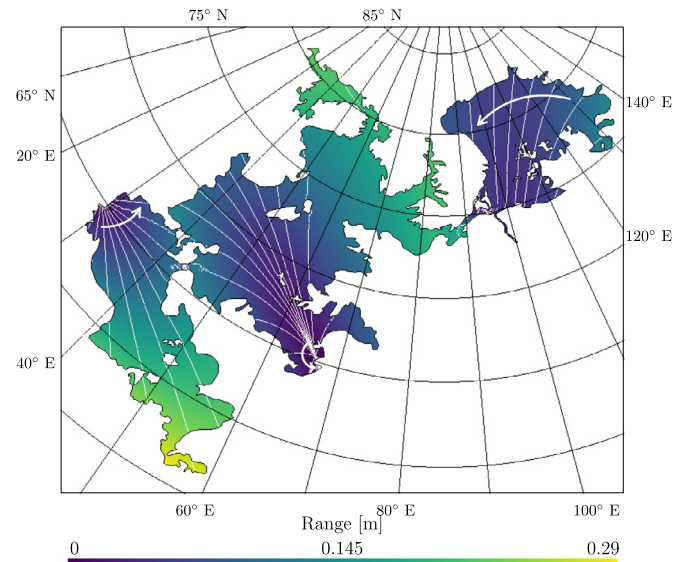


**Fig. 2.** Tidal range (in m) and tidal phase (white lines, with a 15° spacing) of the first tidal component (whose period is 1 TD) in Kraken and Ligeia Maria. The white arrows show the direction of the tide. The tidal range is the surface elevation difference between high tide and low tide. There is an amphidromic point in Kraken 1 (at 65.213°N, 66.459°E) but not in Kraken 2 or Ligeia Mare. The tidal phase at each end of the Seldon and Trevize Fretum are not the same, which results in strong transition in the straits. This is also observed for the tidal range. Such phenomenon suggests independent tidal motion in each basin. The tidal range is maximum in the south-eastern part of Kraken 2.

<sup>2</sup> The amplitude of a tidal component is half of the tidal range which is the difference between high tide and low tide.

tion (see Table 2). In the remainder of this paper, unless otherwise specified, the expressions “tidal range” and “tidal phase” refer to the range and phase of the first tidal component. An amphidromic point of the first tidal component is located in the south-eastern part of Kraken 1, at (65.21°N, 66.47°E) (see Fig. 2). At this location, the most significant component is the third one but the resulting tidal range remains weak: at most  $2.5 \times 10^{-3}$  m. As a consequence, the tides in this basin rotates around this point and the tidal phase ranges from  $-180^\circ$  to  $180^\circ$ . There is no such point in Ligeia Mare or Kraken 2. In Ligeia Mare, the tidal phase is larger than  $-86^\circ$  and smaller than  $19^\circ$  while, in Kraken 2 it ranges from  $-208^\circ$  to  $-52^\circ$ . In both basins, the cotidal lines (lines of constant tidal phase) are not rectilinear, which is due to the friction which is higher in the vicinity of the shoreline and islands as the sea is shallower at these locations.

Fig. 2 shows that, in Kraken 2, the tidal range increases with the distance to a point on the south-western shore and is maximum (0.288 m) at the south-eastern end. In Kraken 1, the tidal range increases with the distance to the amphidromic point and, hence, is higher on the northern shore (maximum: 0.225 m) than in the middle and southern part of the sea. The co-range lines (lines of same tidal range) have an ovoid shape with the longitudinal axis parallel to the maximum width direction and whose center is located at the amphidromic point. In Ligeia Mare, it increases with the distance to a point located on the southern shore of the sea, east of the Ligeia outlet of Trevice Fretum and is maximum (0.14 m) in the south-eastern part of the sea. The tidal motions remain independent of each other in each basin. Indeed, a transition takes place in each strait linking the basins. This transition is sharper in the straits linking Kraken 1 and Kraken 2 than in Trevice Fretum. In the former, there are buffer areas where the tidal range is smaller than elsewhere in the strait, which results in sharp transition in its phase. In the latter, the transition is smoother for both tidal range and phase although it does not take place at the same location (the transition of tidal phase occurs much closer to Ligeia Mare than that of the tidal range). This suggests that, to a large extent, the tidal motion in Kraken 1 and Ligeia Mare can be represented by a sloshing wave mode. Indeed, in these basins, the tidal phase is nearly uniform over large geographical areas while there are strong variations (sometimes by about  $180^\circ$ ) over the straits connecting those basins with Kraken 1 (see Fig. 2).

The norm of the velocity is maximum in the straits such as Trevice Fretum, Seldon Fretum, the small channels next to the latter, and the strait north of Mayda Insula (see Fig. 3). Except for these specific locations, the largest speed is observed nearshore but the fluid velocity is one order of magnitude smaller than in the straits (about 0.027 m/s). In Seldon Fretum, the fluid speed has two maxima located in the middle of the straits, 0.364 m/s and 0.355 m/s, which occur respectively 0.06 *TD* after perikron/apokron while the speed is the lowest (0.08 m/s, which remains larger than everywhere else in the seas, excluding the straits) 0.15 *TD* before perikron/apokron. The current is mainly unidirectional towards Kraken 1 or 2 depending on the period of time (see Fig. 4(a–f)). The transition between two unidirectional flows occurs when the fluid speed at this location is the weakest. Once the flow is unidirectional, it accelerates to reach its maximum speed and then decelerates until it starts turning again. In Trevice Fretum, the maximum speeds, 0.235 m/s and 0.234 m/s, occur respectively 0.3 *TD* after perikron/apokron in the southern part of Trevice Fretum while the speed is the lowest (about 0.065 m/s) 0.07 *TD* after perikron/apokron. As in Seldon Fretum, the flow is mostly unidirectional (see Fig. 4(g–l)) and the flow turns when its speed is the weakest. The period of time during which the flow is unidirectional is longer in Trevice Fretum than in Seldon Fretum. These periods of time are concomitant

with each other as long as the flow is unidirectional in Seldon Fretum.

The fact that the current is almost unidirectional in the Seldon and Trevice Fretum is also shown in Fig. 5: the tidal ellipses<sup>3</sup> of the main tidal component are nearly rectilinear at these locations, which means that there is a fast transition between the two maximum speeds at a given point. Elongated tidal ellipses also occur elsewhere in the Maria but the velocity is much smaller. At locations where the flow speed is smaller than 0.001 m/s (for instance, in the western part of Kraken 2, the south western part of Kraken 1, and the northern part of Ligeia (see Fig. 3)), the ellipses are near circular which indicates that the flow velocity rotates over 1 *TD* instead of being nil during the transition between two directions. The orientation of the flow and, hence, of the tidal ellipses depends on the location. In the straits, the ellipses are aligned with the main axis of the strait while, in their vicinity, they point at the nearest mouth of the strait. Offshore, where the speed is larger than 0.001 m/s, the main axis of the ellipses is aligned with the streamlines at perikron/apokron (see Fig. 3).

The tidal forcing studied in this paper does not seem to generate resonance in the northern seas (at least during the 15 *TD* studied). Nevertheless, it does not mean that eigenmodes of the northern seas could not be excited by other phenomena. In order to study the eigenmodes, we performed a discrete modal analysis of the Discontinuous Galerkin solution of the linear shallow water equations following the method of Bernard et al. (2008). The eigenvalues and eigenvectors are computed by means of the `linalg.eig` function of `scipy` package of python which solves the generalized eigenvalue problem  $M \frac{dU}{dt} = AU$  where  $M$  is the mass matrix,  $A$  is the discontinuous galerkin discretisation of the linear shallow water space operators for the domain, and  $U = (\eta, u, v)$  is the solution. The periods of the eigenmodes range from  $2.55 \times 10^{-3}$  *TD* to 15171 *TD*. Nevertheless, most of the eigenmodes (90%) have a period smaller than 25 *TD* (see Fig. 6(a)). Some of the eigenmodes have a period close to 1 *TD* but these eigenmodes consist in localized modifications of the sea surface elevation in some of the small bays, along the northern shore of Ligeia Mare or near the islands of Kraken 2 and Ligeia Mare. These localized phenomena do not play a significant role in the global tides of the northern seas and these eigenmodes are not noticeable while looking at the tidal motion. Some of the eigenmodes correspond to phenomena such as coastal trapped waves or funnel shaped waves but their resonance frequency is not excited by the tides. A complete discussion of the northern seas eigenmodes is of interest but beyond the scope of this article.

In Kraken 1, 2, and Ligeia Mare, the Rossby radius of deformation ( $R = \frac{\sqrt{gh}}{f}$  where  $g = 1.352 \text{ m/s}^2$  is the mean gravitational acceleration at Titan’s surface,  $h$  is the depth, and  $f$  is the Coriolis parameter) ranges are respectively [91.3, 1776.3] km, [98.5, 1938.2] km, and [93.5, 1655.3] km. These values are larger than the characteristic length scale of the basins except for areas near the shore where the seas are shallower. This means that rotating shallow water waves such as Kelvin waves could appear near shore,  $R$  being smaller than the characteristic length scale at these locations. Other coastal trapped waves such as the edge waves could occur in the northern seas while continental shelf waves are ruled out because there is no shelf. Some of the eigenmodes of the northern seas correspond to such coastal trapped waves but they are not excited by the tides as their periods are much smaller than the tidal period. Nevertheless, coastal trapped waves could appear due to other forcings such as the wind but this is beyond the scope of this article. Furthermore, the evolution of the sea sur-

<sup>3</sup> A tidal ellipse is the locus of the end of the velocity vector associated with one tidal component over a tidal period at one point.

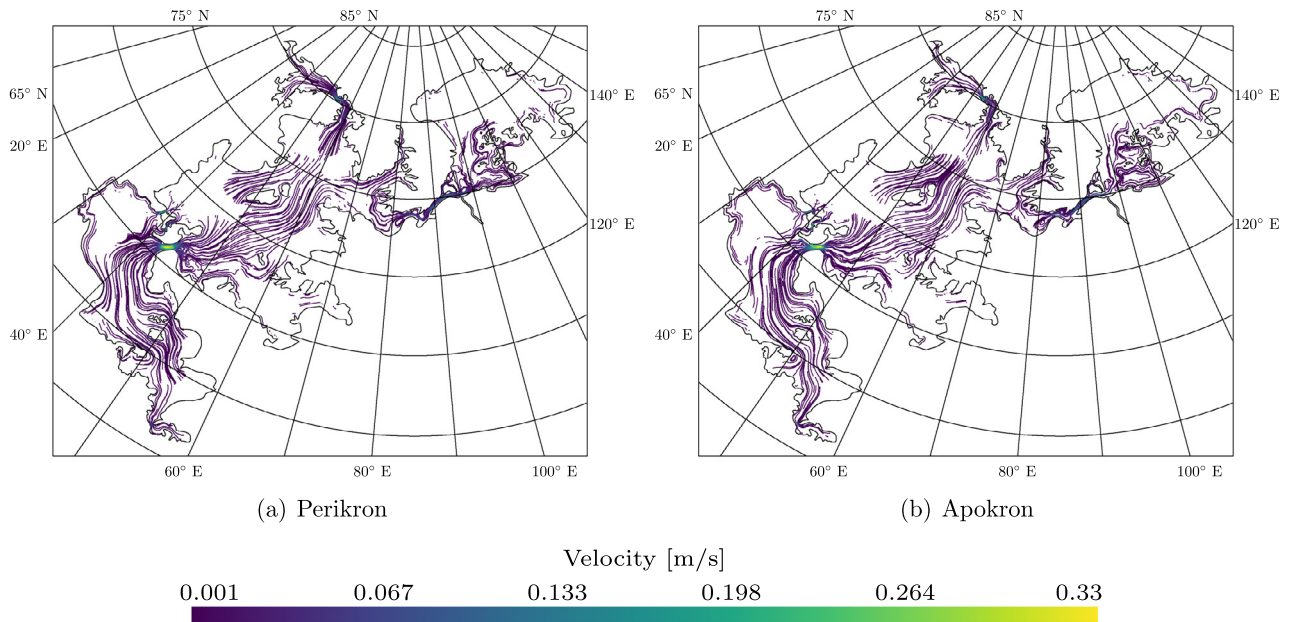


**Fig. 3.** Tidal current streamlines at Perikron (a) and Apokron (b). The empty areas correspond to areas where the predicted velocity field magnitude is smaller than 0.001 m/s. At these periods, the main current pattern is a flux going from the south-eastern part of Kraken 2 towards the north of Kraken 1 and from Moray Sinus towards Ligeia Mare (Panel (b)) or in the opposite direction (Panel (a)).

face elevation over one tidal period does not show evidence for any coastal trapped waves (see the video of the tidal motion over 1  $TD$  in additional content). Such waves are, hence, unlikely, unless they have a period smaller than  $0.05 TD$  ( $\sim 6.9 \times 10^4$  s) (which is the numerical time step) or larger than  $0.5 TD$  ( $\sim 6.9 \times 10^5$  s) or they occur on a really small spatial scale. Topographic planetary waves could occur if  $|\nabla_h H| \geq HR_0$  (LeBlond and Mysak, 1978) where  $H$  is the depth,  $R_0 = R \tan \phi_0$  ( $R$  is Titan radius and  $\phi_0$  is the latitude), and  $|\nabla_h H| \sim 0.002$  is the bathymetry gradient. This condition being never encountered with the bathymetry implemented, such waves are not expected. Offshore, the shallow water waves phase speed tends to  $c = \sqrt{gh}$  and to be non dispersive. In Trevize and Seldon Fretum, capillary waves could occur—thus tidal current could generate surface roughness detectable in radar observations. Indeed, Hayes et al. (2013) calculated a speed for capillary waves (3 cm wavelength) of 0.11 m/s, which is lower than the flow velocity in those straits. Other phenomena, which could not be detected by spacecraft instrument, such as surface gravity waves and turbulence, could also occur in these seas and might play a role in the transfer of energy and momentum to these waves.

It is noteworthy that the system of two basins connected by a channel is a classic Helmholtz oscillator. A terrestrial example of such behaviour is the identification of a 48–72 hr periodicity in currents through the Straits of Mackinac, between the Great Lakes, Michigan and Huron (Anderson and Schwab, 2013). The two major Kraken basins and Seldon Fretum form an analogous system. The natural period can be calculated (Eq. 8 of Anderson and Schwab (2013)) from the channel cross-section ( $A_c \sim 0.2$  km<sup>2</sup>, for  $\sim 10$  m depth), the area of the basins ( $A_{K1} \sim 2.4 \times 10^5$  km<sup>2</sup> and  $A_{K2} \sim 1.3 \times 10^5$  km<sup>2</sup>), the channel length  $l = 40$  km and gravity  $g = 1.352$  m/s<sup>2</sup> as  $T = 2\pi \sqrt{\frac{l}{A_c g \left( \frac{1}{A_{K1}} + \frac{1}{A_{K2}} \right)}}$ . With these values, the predicted period is about 8.8 Earth days. As this period is not an integer divisor of the tidal period, it would take several tidal cycles to observe any resonance phenomena with the tides. The Ligeia-Trevize-Kraken system has an even longer period (about 18.7 Earth days) and would be more heavily damped by the long tortuous channel, so the Helmholtz mode will be insignificant there. Other

possible resonance phenomenon could be the quarter wavelength resonance. The latter can be observed on shelves in the Earth ocean. The speed of long waves is given by  $c \sim \sqrt{gh}$ . For a tidal period of 1  $TD$  (about 15.95 Earth days), the resulting quarter wavelength width ranges from 283 km nearshore up to 5500 km at the maximum depth. This increase is not linear. For instance, the quarter wavelength width is higher than 1400 km at 1.7 km offshore. Consequently, such resonance phenomenon is unlikely in Titan's northern seas.

### 3.2. Fluid exchanges between the basins

In this sub-section, we focus on the tidally induced fluid exchanges between Ligeia Mare and Kraken Mare and between both basins of Kraken Mare. There are much more liquid exchanges between both basins of Kraken Mare than between Kraken Mare and Ligeia Mare: the maximum volumetric flow rate through Seldon Fretum is about three times larger than in Trevize Fretum (see Fig. 7) and the total volumetric flow rate through Seldon Fretum (in one way or another) over one Titan day is 32.7 km<sup>3</sup>/ $TD$  while it is 10.5 km<sup>3</sup>/ $TD$  in Trevize Fretum. The former matches the semianalytic estimate of Lorenz et al. (2014); they considered a wedge-like volume of liquid of 10–30 km<sup>3</sup> in each half period. Fig. 7 shows that there is an asymmetry in the flow rate through both straits: it does not behave as a sinusoid. Indeed, the behaviour of the volumetric flow rate is not the same at its maximum and at its minimum. This is due to the fact that the flow rate in the straits does not only depend on the velocity but also on the sea surface elevation at this location. For instance, in Trevize Fretum, the flow rate increases faster after its minimum than after its maximum (the slope of the graph is steeper). This can be linked to the fact that the sea surface elevation is positive in Trevize Fretum when the volumetric flow rate is maximum. This larger total depth of liquid results in a slower decrease of the volumetric flow rate when the velocity decreases. Despite this asymmetry, the daily average is nil. The volumetric flow rates explain the smaller volume variation in Ligeia Mare. Indeed, the latter is about three times larger in both basins of Kraken Mare than in Ligeia Mare (see Fig. 8).

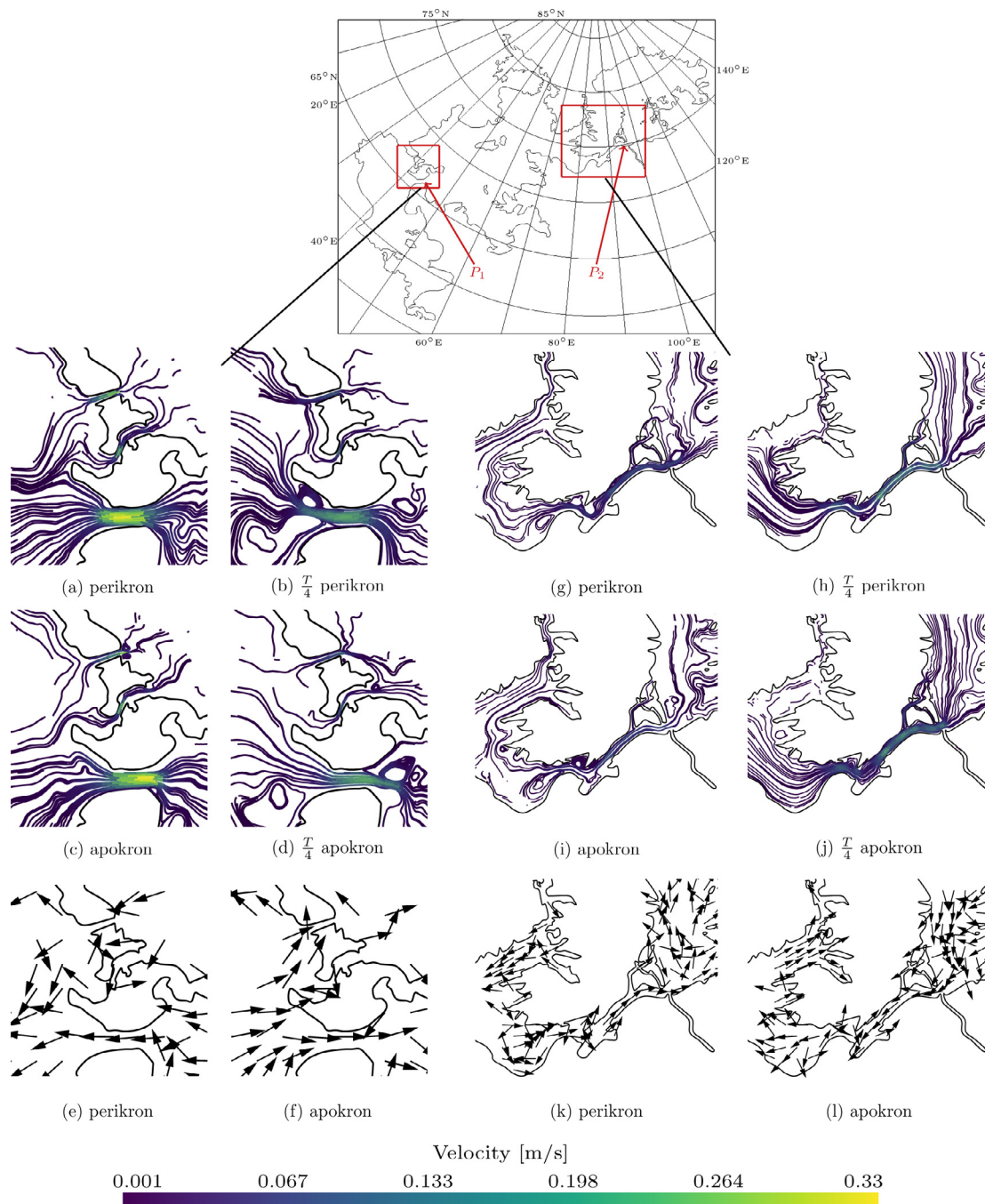


**Fig. 4.** Streamlines (a, b, c, d, g, h, i, j) and orientation (e, f, k, l) of the tidal current (in m/s) in Seldon and Trevize Fretum at four times of day: Perikron (a, e, h),  $T/4$  after Perikron (b, i), Apokron (c, f, j), and  $T/4$  after Apokron (d, k). The fluid speed is maximum (0.364 m/s) in Seldon Fretum 0.06  $TD$  after perikron. The other areas where the speed is high are, in first instance, the other straits and, in second instance, the nearshore regions corresponding to specific shapes in the shoreline such as cape, peninsula and bay. The velocity in the strait is unidirectional for most of a Titan day (see Panels (e, f, k, l)).

Consequently, there is a strong correlation between volume variation in Kraken 1 and Kraken 2: the volume variation is maximum in one basin soon after/before the minimum in the other and vice versa (see Fig. 8). This can be explained by the fact that the tidal forcing magnitude is more significant in the surroundings of Seldon Fretum than near Trevize Fretum and by the shape of the straits: Trevize Fretum is much more elongated than Seldon Fretum and the small channels next to Seldon Fretum allow for additional liquid exchanges. The volume variation of each basin behaves as a sinusoid whose period is 1  $TD$ . Although being significant, the volume variation is quite weak with respect to the

volume of the basins. Indeed, for this bathymetry, the total volume of Ligeia Mare, Kraken 1 and Kraken 2 are respectively about 4500 km<sup>3</sup>, 13000 km<sup>3</sup> and 7200 km<sup>3</sup> while the maximum volume variations over a Titan day predicted by our model with these parameters are about 2.5 km<sup>3</sup>, 8.9 km<sup>3</sup>, and 9.2 km<sup>3</sup> respectively.

We also studied the fluid exchanges between the basins and Maria over a period of time of 150  $TD$  (about 6.55 Earth years or 0.22 Titan years) by means of a passive tracer: the tracer concentration is set to 1 in Ligeia Mare and Kraken 2 and to 0 in Kraken 1. This means that wherever the tracer is larger than 0 in Kraken 1 (or smaller than 1 in the others basins), there is some

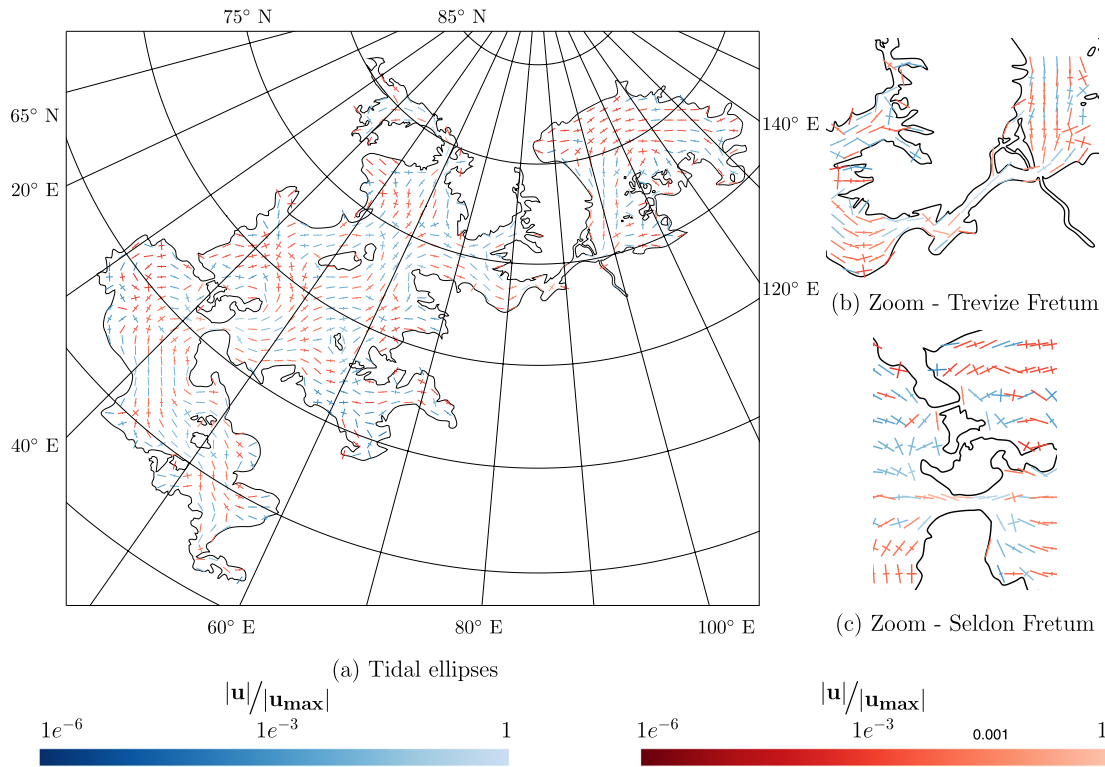


**Fig. 5.** Major and minor axes of the tidal ellipses in the northern seas (Panel (a)), Trevize Fretum (Panel (b)) and Seldon Fretum (Panel (c)). The tidal ellipses represent the orientation of the first tidal component of the current over a whole period. Red and blue ellipses respectively indicate an anti-clockwise/clockwise rotation while the color scales with the magnitude of the maximum velocity over 1 TD. The smaller the minor axis, the more elongated the ellipses and the more unidirectional the velocity. (For interpretation of the references to color in this figure legend, the reader is referred to the web version of this article).

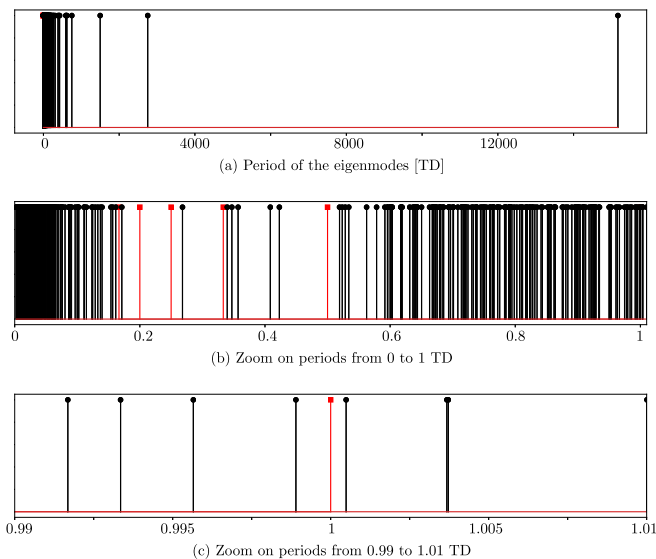


**Fig. 6.** Periods of the northern seas eigenmodes (Panel (a), in TD) with a zoom from 0 to 1 TD (Panel (b)) and from 0.99 to 1.01 TD (Panel (c)). The tidal period and its first fifth integer divisors are in red. (For interpretation of the references to color in this figure legend, the reader is referred to the web version of this article).

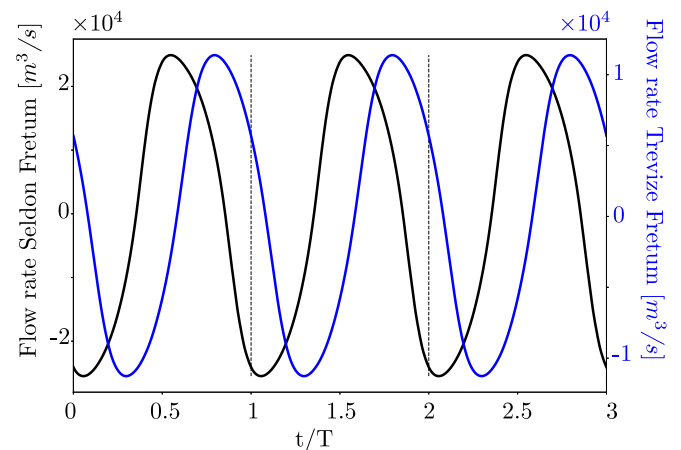


**Fig. 7.** Volumetric flow rate through Seldon (black line) and Trevize Fretum (blue line) over three Titan days. In Seldon and Trevize Fretum, it is respectively positive towards Kraken 1 and Ligeia Mare. The volumetric flow rate through the former is about three times larger than that through the latter. The net difference over 1 TD is  $0 \text{ km}^3$ . (For interpretation of the references to color in this figure legend, the reader is referred to the web version of this article).

liquid originating from the adjacent basin(s). Such volumes grow over time. They grow faster in Kraken Mare than in Ligeia Mare. For instance, after 150 TD, at least 1% of the liquid at one location is originating from another basin in most of Kraken Mare (see Fig. 9(a)). The areas where this is not the case are almost enclosed bays such as that west of Mayda Insula. On the contrary, in Ligeia,

there are some traces of liquid originating from Kraken Mare only in the southern part of the sea, near Trevize Fretum. If we look at higher thresholds, we can see that the liquid exchanges between Ligeia Mare and Kraken Mare remains confined to Trevize Fretum and the small channels at Ligeia outlet. On the other side, there is a wide area (about half of the basin) in both basins of Kraken Mare where at least 5% of the liquid is originating from the other

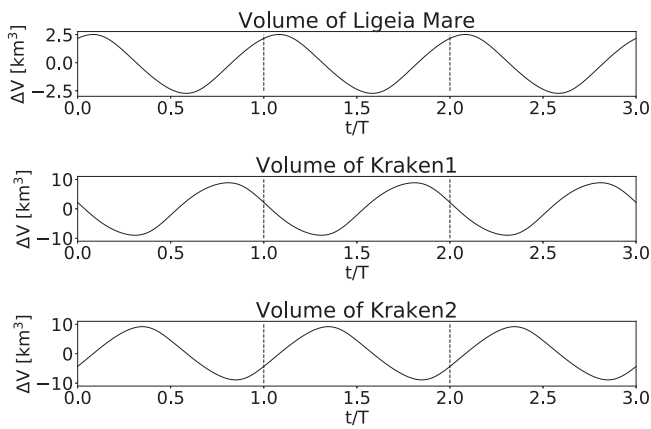


**Fig. 8.** Volume variation in the basins of Kraken and Ligeia Maria over three Titan days. The variation is larger in both basins of Kraken Mare than in Ligeia Mare and the total variation of each basin over a Titan day is nil.

basin, which is due to the much more significant liquid exchanges through Seldon Fretum (see Fig. 9(b)). The area where at least 10% of the liquid is originating from the other basin remains located near Seldon Fretum in Kraken 1 while it spreads over the western part of Kraken 2 (see Fig. 9(c)). This can be due to the smaller volume of liquid and smaller area of Kraken 2 (about 54% of the volume of Kraken 1). Unless a precipitation event (which is unlikely in Kraken 2 and in the southern region of Kraken 1) or an evaporation rate peak (which seems to occur during the spring) occurs, our model gives a good approximation of the tidally induced liquid exchanges between the basins of Kraken Mare. Indeed, the density driven circulation predicted in Seldon Fretum by Tokano and Lorenz (2016) are either insignificant (for the thermally forced circulation) or at least one order of magnitude smaller (see Fig. 14a of Tokano and Lorenz (2016)) than the tidally induced flow (for precipitation/evaporation driven flows). Furthermore, the former occurs on a much larger time scale than the diurnal time scale of the tides. On the other hand, there could be a more significant difference in composition between Ligeia and Kraken Maria (Lorenz, 2014). As the shape of the strait almost reduces the tidal flow to a back and forth motion, a significant density gradient in the strait could modify the flow in Trevize Fretum and, hence, the liquid exchanges. But studying this is beyond the scope of the present article. Furthermore, other factors could modify these results. For example, in the case of a pure tidal flow in and out of Ligeia Mare through Trevize Fretum, then the same parcel of liquid is washed back and forth and the net mixing is small: a parcel of liquid comes through the channel and sits at the mouth, then is sucked back through. However, if there is, for instance, a strong wind-generated gyre in Ligeia Mare, then whatever Kraken Mare liquid is hosed out of Trevize Fretum into Ligeia Mare is quickly swept away and mixed into Ligeia Mare, and what is sucked back into Trevize Fretum is now mostly Ligeia Mare liquid, not the previously Kraken parcel. Consequently, we can only assess that the variation of liquid composition observed in Moray Sinus (Hayes et al., 2011) with respect to Kraken Mare cannot be explained by tidally induced liquid exchanges over a time scale smaller than 150 TD. This variation could be related to liquid exchanges with Ligeia Mare over a much longer period or to liquid exchanges interacting with wind gyre(s) (or similar phenomenon) at one (at least) of Trevize Fretum outlets.

### 3.3. The canyons of Ligeia Mare

In this section, we investigate the tidal current and sea surface elevation in the canyons studied by Poggiali et al. (2016). We show that the tides do not play a significant role in filling these

canyons. As no information is available about the liquid depth in these canyons, the bathymetry is derived similarly to that of Ligeia Mare. Near Vid Flumina, it results in a maximum depth of 2.3 m, the mean depth being about 1 m while the maximum depth is about 6.5 m near Xhantus Flumen. This bathymetry does not take into account the slope of the bottom of the canyons, the latter being unknown: Poggiali et al. (2016) predicted that the liquid surface is at the same level as in Ligeia Mare with an error of about 0.7 m.

The maximum sea surface elevation in the canyons is about 0.034 m, which does not significantly modify the liquid depth at this location and cannot be detected by any Cassini instrument. At the time of the flyby analysed by Poggiali et al. (2016) (T91, at a true anomaly of  $\nu = 69^\circ$ ), the tide was high in the canyons: the sea surface elevation was between 0.009 m and 0.02 m in the canyons near Vid Flumina while it was between 0.027 m and 0.031 m in those located next to Xanthus Flumen. Unfortunately, such variations are too small to be observed by means of the Radar whose precision along the vertical axis is about 0.7 m (Poggiali et al., 2016). There is no discontinuity between the tides in the canyons and in Ligeia Mare: the liquid motion in the canyons is induced by the tides of Ligeia Mare. In both canyons, the only significant tidal component is the first harmonic (see Fig. 10).

The maximum velocity in the canyons near Vid Flumina is 0.064 m/s and occurs at the mouth of the dendritic network, where the canyon is narrow. Except for this location and at the mouth of the southern canyon, the speed is lower than 0.04 m/s. In the canyon near Xanthus Flumen, the speed is lower than 0.012 m/s.

In the light of such predictions and as we do not take into account the slope in the canyon, it is highly unlikely that the liquid filling these canyons is due to the tides. Nonetheless, those conclusions may be put into question if there are significant discrepancies between the bathymetry implemented in the numerical model and the real bathymetry.

### 3.4. Moray sinus and the “Magic Islands” phenomenon

In this section, we will detail the tidal response of the northern seas in regions where transient features were observed and in a bay west of Trevize Fretum, Moray Sinus. The “Magic Islands” phenomenon was observed both in Kraken and Ligeia Maria. Nevertheless, Hofgartner et al. (2016) suggested that, in Ligeia, the phenomenon is independent from the diurnal tide. Consequently, it is not of a particular interest to study accurately these areas.

In Kraken Mare, the “Magic Island” was observed at (73°N, 55°E) between T91 and T104 flybys. The true anomaly of Titan during these flybys was 69° and 246° respectively, which correspond to a variation of 177°, almost half a Titan day. Consequently, diurnal phenomenon such as the tides cannot be ruled out. In this area, tidal components other than the diurnal one are not significant and, hence, can be disregarded. The sea surface elevation variation between both flybys is about 0.1 m, which is too small to explain the phenomenon. The tidal currents in this area are weaker than 0.029 m/s (the maximum occurs near the shores of the nearby island), which is smaller than the speed for capillary waves (3 cm wavelength) calculated by Hayes et al. (2013) (0.11 m/s).

In Moray Sinus, the bathymetry is amphitheater-shaped with a maximum depth (45 m) at the inlet. The main tidal component is diurnal and the tidal range ranges from 0.17 to 0.225 m. The flow is really weak except in the narrow part at the northern end of Moray Sinus where it can reach 0.058 m/s. In both areas, no capillary waves are expected, the tidal flow being too small. Nevertheless, with different bathymetry assumptions, the flow speed could be higher. In this connection, we note that the speed for capillary waves (3 cm wavelength) calculated by Hayes et al. (2013) could be reached—thus tidal currents could conceivably generate surface

**Table 3**

Sea surface elevation ( $\eta$ ), tidal current ( $u$ ), tidal range ( $\Delta\eta$ ), maximum volume variation ( $\Delta V$ ), and liquid exchanges through a strait over one Titan Day for the various values of the parameters.  $\gamma_2$  is the attenuation factor,  $H$  is the depth (constant) of Trevize Fretum,  $\alpha$  is the scaling factor for the bathymetry, and  $n$  is Manning's coefficient. S, T, L, K1, and K2 subscripts respectively refer to Seldon Fretum, Trevize Fretum, Ligeia Mare, Kraken 1, and Kraken 2. The reference case (bold text) corresponds to  $\gamma_2 = 0.1$ ,  $n = 0.03 \text{ ms}^{-1/3}$ , and a bathymetry scaling with the distance to the shore.

|                                 | $\eta_{max}$<br>[m] | $\ u\ _S$<br>[m/s] | $\ u\ _T$<br>[m/s] | $\Delta\eta_{max}$<br>[m] | $\Delta V_L$<br>[km <sup>3</sup> /TD] | $\Delta V_{K1}$<br>[km <sup>3</sup> /TD] | $\Delta V_{K2}$<br>[km <sup>3</sup> /TD] | $\Delta V_S$<br>[km <sup>3</sup> ] | $\Delta V_T$<br>[km <sup>3</sup> ] |
|---------------------------------|---------------------|--------------------|--------------------|---------------------------|---------------------------------------|--|--|------------------------------------|------------------------------------|
| $\gamma_2 = 0.05$               | 0.086               | 0.242              | 0.172              | 0.168                     | 1.8                                   | 6.2                                      | 5.9                                      | 21.103                             | 7.523                              |
| $\gamma_2 = 0.1$ <sup>a</sup>   | <b>0.145</b>        | <b>0.364</b>       | <b>0.235</b>       | <b>0.288</b>              | <b>2.5</b>                            | <b>8.9</b>                               | <b>9.2</b>                               | <b>32.749</b>                      | <b>10.501</b>                      |
| $\gamma_2 = 0.2$                | 0.247               | 0.523              | 0.32               | 0.492                     | 3.6                                   | 12.3                                     | 13.7                                     | 48.712                             | 14.642                             |
| $\gamma_2 = 0.3$                | 0.342               | 0.64               | 0.385              | 0.678                     | 4.6                                   | 14.8                                     | 17.1                                     | 60.661                             | 17.847                             |
| $H = 10 \text{ m}$              | 0.143               | 0.357              | 0.202              | 0.285                     | 3.9                                   | 8.6                                      | 9  | 32.071                             | 16.133                             |
| $H = 20 \text{ m}$ <sup>b</sup> | 0.162               | 0.342              | 0.304              | 0.331                     | 10.8                                  | 8.2                                      | 8.8                                      | 30.955                             | 44.151                             |
| $H = 50 \text{ m}$ <sup>b</sup> | 0.223               | 0.434              | 0.211              | 0.446                     | 15.7                                  | 7.6                                      | 11.24                                    | 39.714                             | 63.488                             |
| $n = 0.01 \text{ sm}^{-1/3}$    | 0.184               | 0.595              | 0.523              | 0.354                     | 6                                     | 14.5                                     | 12.74                                    | 43.834                             | 22.854                             |
| $n = 0.02 \text{ sm}^{-1/3}$    | 0.165               | 0.448              | 0.332              | 0.326                     | 3.6                                   | 11.6                                     | 11.3                                     | 39.677                             | 14.574                             |
| $n = 0.04 \text{ sm}^{-1/3}$    | 0.129               | 0.293              | 0.178              | 0.258                     | 2                                     | 6.9                                      | 7.4                                      | 26.763                             | 7.987                              |
| $n = 0.05 \text{ sm}^{-1/3}$    | 0.118               | 0.241              | 0.144              | 0.235                     | 1.6                                   | 5.6                                      | 6.2                                      | 22.267                             | 6.413                              |
| $n = 0.06 \text{ sm}^{-1/3}$    | 0.11                | 0.203              | 0.12               | 0.22                      | 1.3                                   | 4.7                                      | 5.2                                      | 18.946                             | 5.352                              |
| $2\alpha$ <sup>c</sup>          | 0.179               | 0.269              | 0.273              | 0.352                     | 3.4                                   | 14.6                                     | 13.4                                     | 47.193                             | 14.343                             |
| $0.5\alpha$ <sup>d</sup>        | 0.099               | 0.258              | 0.219              | 0.192                     | 1.2                                   | 2.7                                      | 3.3                                      | 11.806                             | 4.385                              |

<sup>a</sup> Reference case (i.e.  $\gamma_2=0.1$ ,  $n = 0.03 \text{ sm}^{-1/3}$  and no bathymetry modification).

<sup>b</sup> In these cases, the maximum elevation occurs in Ligeia Mare.

<sup>c</sup> In this case, the bathymetry in Kraken Mare is computed with a scaling factor doubled.

<sup>d</sup> In this case, the bathymetry in Kraken Mare is computed with a scaling factor divided by 2

**Table 4**

Location of potential amphidromic point(s) for the various values of the parameters.  $\gamma_2$  is the attenuation factor,  $H$  is the depth (constant) of Trevize Fretum,  $\alpha$  is the scaling factor for the bathymetry, and  $n$  is Manning's coefficient. The reference case (bold text) corresponds to  $\gamma_2 = 0.1$ ,  $n = 0.03 \text{ ms}^{-1/3}$ , and a bathymetry scaling with the distance to the shore.

|                                 | Amphidromic Point<br>in Kraken 1 | Amphidromic Point<br>in Kraken 2 |
|---------------------------------|----------------------------------|----------------------------------|
| $\gamma_2 = 0.05$               | (64.06°N, 65.102°E)              | –                                |
| $\gamma_2 = 0.1$ <sup>a</sup>   | <b>(65.213°N, 66.459°E)</b>      | –                                |
| $\gamma_2 = 0.2$                | (67.391°N, 64.197°E)             | (64.171°N, 32.143°E)             |
| $\gamma_2 = 0.3$                | (68.418°N, 62.529°E)             | (63.897°N, 33.905°E)             |
| $H = 10 \text{ m}$              | (66.695°N, 62.16°E)              | –                                |
| $H = 20 \text{ m}$ <sup>b</sup> | (70.056°N, 44.491°E)             | –                                |
| $H = 50 \text{ m}$ <sup>b</sup> | –                                | –                                |
| $n = 0.01 \text{ sm}^{-1/3}$    | –                                | –                                |
| $n = 0.02 \text{ sm}^{-1/3}$    | (65.032°N, 63.27°E)              | –                                |
| $n = 0.04 \text{ sm}^{-1/3}$    | (66.57°N, 65.686°E)              | (64.302°N, 31.032°E)             |
| $n = 0.05 \text{ sm}^{-1/3}$    | –                                | (63.927°N, 33.202°E)             |
| $n = 0.06 \text{ sm}^{-1/3}$    | –                                | (63.721°N, 34.711°E)             |
| $2\alpha$ <sup>c</sup>          | (67.347°N, 48.643°E)             | –                                |
| $0.5\alpha$ <sup>d</sup>        | (70.3506°N, 57.958°E)            | (63.15°N, 38.5°E)                |

<sup>a</sup> Reference case (i.e.  $\gamma_2=0.1$  and no bathymetry modification).

<sup>b</sup> In these cases, the maximum elevation occurs in Ligeia Mare.

<sup>c</sup> In this case, the bathymetry in Kraken Mare is computed with a scaling factor doubled.

<sup>d</sup> In this case, the bathymetry in Kraken Mare is computed with a scaling factor divided by 2.

roughness detectable in radar observations in both Moray Sinus and where the “Magic Island” was observed.

#### 4. Influence of the model parameters

In this section, a sensitivity analysis to the poorly constrained parameters  $\gamma_2$ , the depth of Trevize Fretum, the bathymetry of Kraken Mare, and the bottom friction is conducted. We also present our results when a bathymetry mimicking that shown in Fig. 9a of Hayes (2016) is used in Ligeia Mare. The main results are summarised in Tables 3 and 4. The reference values are  $\gamma_2 = 0.1$ ,  $n = 0.03 \text{ sm}^{-1/3}$  and a bathymetry scaling with the distance to the shore, which corresponds to the results presented in Section 3.

##### 4.1. Influence of the attenuation factor $\gamma_2$

We discuss the influence of the attenuation factor  $\gamma_2$  on the tidal response in Ligeia and Kraken Maria. In order to take into account the wide range of values of Love numbers found in the literature (see Section 2.2), we studied  $\gamma_2$  for values ranging from 0.05 to 0.3. The maximum tidal range is an increasing function of the attenuation factor within the studied range (see Fig. 11). The maximum surface elevation (and tidal range) occurs at the same location and at the same time (0.31 TD after perikron) whatever the value of  $\gamma_2$  (see the video entitled “Northern\_seas\_sse\_gamma2” in the additional content), which is not the case for the velocity. Indeed, although the maximum speed remains located in Seldon Fretum, the time slightly varies with  $\gamma_2$ : the higher  $\gamma_2$ , the later the maximum speed occurs (there is a time lag of 0.045 TD between  $\gamma_2 = 0.05$  and 0.3). The opposite is observed in Trevize Fretum: the higher  $\gamma_2$ , the earlier the maximum speed occurs in the strait. In Seldon and Trevize Fretum, the maximum speed behaves like a square root with respect to  $\gamma_2$ : it increases and seems to tend towards a constant value (see Fig. 11). The increase is larger in Seldon Fretum than in Trevize Fretum: the speed is respectively multiplied by 2.64 and 2.24 between  $\gamma_2 = 0.05$  and 0.3. This may be interpreted as follows: at some point, the geometry of the strait prevails the tidal forcing concerning the maximum speed. In the seas, the speed also increases with  $\gamma_2$  but it remains of the same order of magnitude whatever the value of  $\gamma_2$  except at some specific locations such as capes, peninsula, islands or smaller straits. The flow orientation can change locally when  $\gamma_2$  varies but the global patterns of the flow remain identical.

The most significant changes induced by  $\gamma_2$  variations are the modifications in the phase and range of the first tidal component. For instance, for  $\gamma_2 \geq 0.2$  a second amphidromic point appears (see Fig. 12(b)). It is located in the south-western part of Kraken 2. The existence and the position of such amphidromic points are clearly related to the value of  $\gamma_2$ . Between  $\gamma_2 = 0.05$  and  $\gamma_2 = 0.3$ , the amphidromic point moves by about 201 km in Kraken 1 while, between  $\gamma_2 = 0.2$  and  $\gamma_2 = 0.3$ , it moves by about 37 km in Kraken 2. In Kraken 1, the amphidromic point moves North-westwards as  $\gamma_2$  increases except for the transition between  $\gamma_2 = 0.05$  and  $\gamma_2 = 0.1$  where it moves North-eastwards. In Kraken 2, it moves south-eastwards (see Table 4). As a consequence of this displacement,

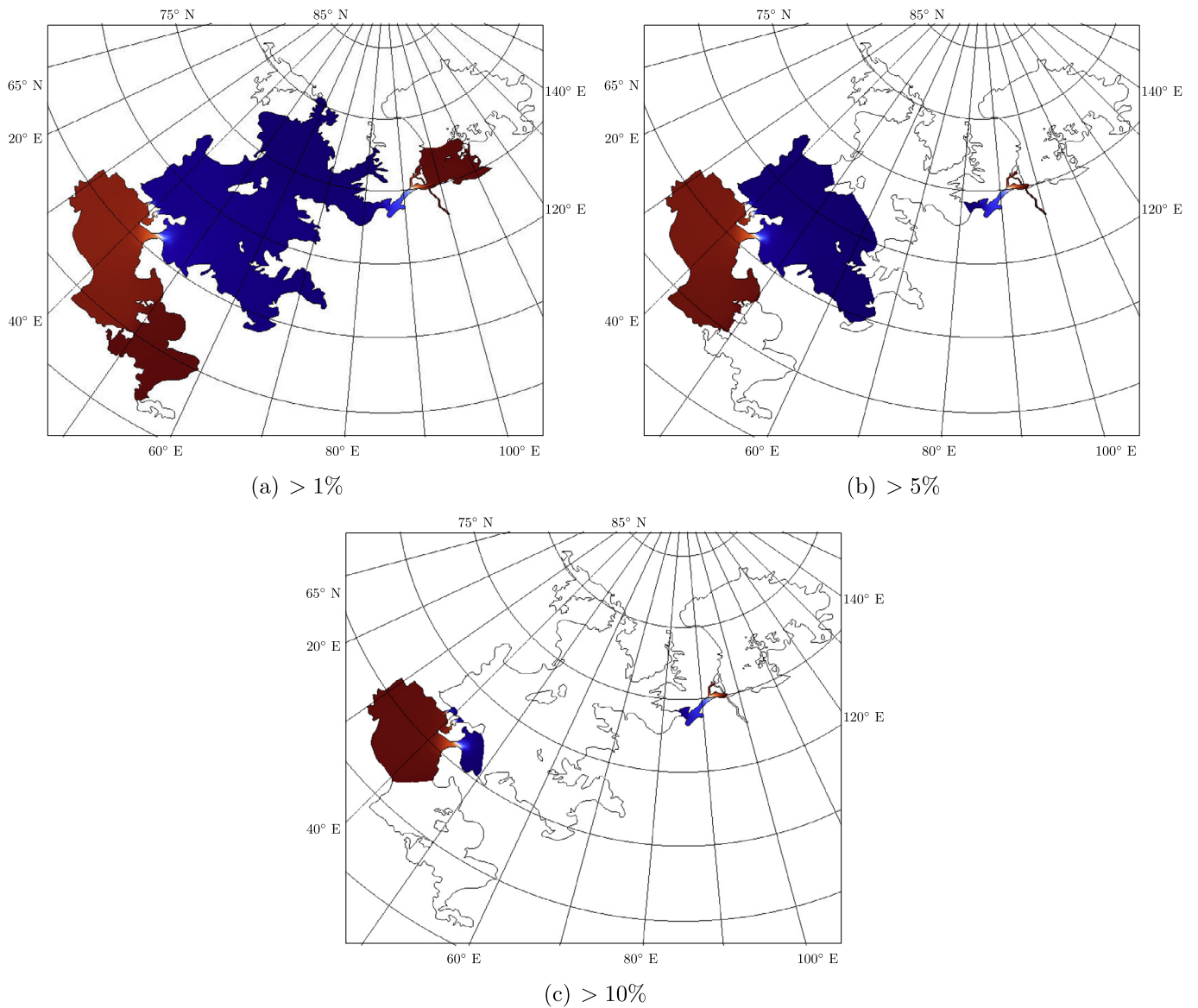


**Fig. 9.** Tracing experiment to illustrate the fluid exchanges between the basins of the northern Maria. The colored areas are the regions where at least 1% (Panel (a)), 5% (Panel (b)), and 10% (Panel (c)) of the liquid comes from the adjacent basin(s) after 150TD. The mixing of Ligeia Mare is very slow while it is fastest in Kraken 2. (For interpretation of the references to color in this figure legend, the reader is referred to the web version of this article).

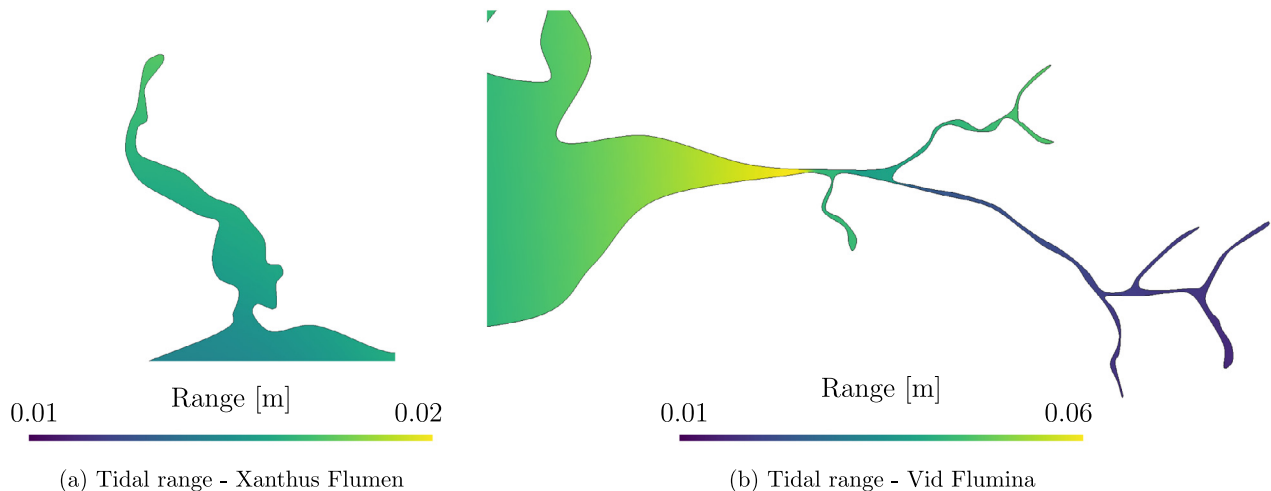


**Fig. 10.** Tidal range in canyons near Xanthus flumen (a) and near Vid Flumina (b) for the reference case. The areas shown in these figures correspond to red rectangles D and C in Fig.1. (For interpretation of the references to color in this figure legend, the reader is referred to the web version of this article).

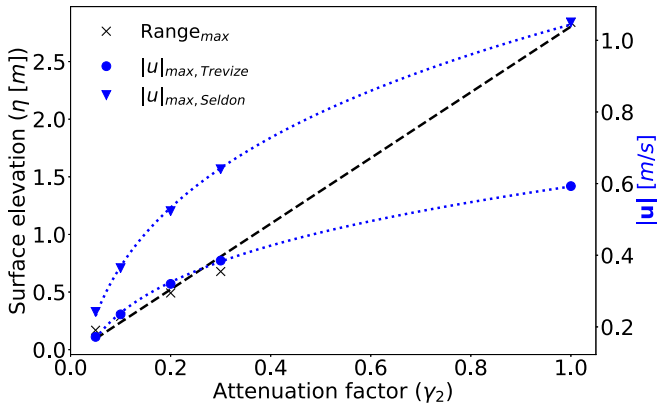


**Fig. 11.** Maximal tidal range (cross, in m) and maximum fluid speed in Trevice (circle, in m/s) and Seldon (triangle, in m/s) Fretum as function of the attenuation factor  $\gamma_2$ . The dashed and dotted lines are respectively a linear and a quadratic mean square root approximation.

the tidal range can locally decrease although  $\gamma_2$  is increasing. The shape of the corange lines does not change with  $\gamma_2$ : it remains an ovoid centred on the amphidromic point. Consequently, their orientation locally varies with  $\gamma_2$  as the amphidromic point moves. It also results in much stronger variations (in tidal range and phase) in the strait linking both basins of Kraken Mare. The variations of the tidal phase and displacement of these amphidromic points are due to a side effect of the variation of  $\gamma_2$ : the resulting modifications of liquid exchanges and, hence, the volume variation of each basin (see Fig. 14). Indeed, if we look at an enclosed basin (i.e. without liquid exchange with others basins), there is no variation of the tidal phase or amphidromic point displacement when  $\gamma_2$  varies.

Variations of  $\gamma_2$  strongly modify the amount of liquid exchanges between the basins through Seldon and Trevice Fretum (see Fig. 13). The volumetric flow rate over a Titan day is respectively multiplied by 2.87 and 2.37 between  $\gamma_2 = 0.05$  and  $\gamma_2 = 0.3$  (see Table 3) and it does not occur at the same time of the day, which is consistent with the behaviour of the velocity field. These effects are also noticeable when looking at the volume variation over the basin (i.e. Kraken 1, Kraken 2 and Ligeia Mare): the larger  $\gamma_2$ , the larger the volume variation (see Fig. 14). For instance, the maximum volume variation in Kraken 1, Kraken 2 and Ligeia Mare are multiplied by 2.37, 2.89 and 2.55 between  $\gamma_2 = 0.05$  and  $\gamma_2 = 0.3$ . A small time lag in volume variation is also observed between each value of  $\gamma_2$ . Except for  $\gamma_2 = 0.05$ , when it occurs in Kraken 1, the maximum volume variation occurs in Kraken 2 (Fig. 14).

These results allow us to assess that the attenuation factor has not only an impact on the surface elevation and the velocity (magnitude and orientation) at a given point but it also affects the tidal phase and the global behaviour of the tides. This proves that the deformability of Titan's surface has a significant influence on the tides.

#### 4.2. Influence of the depth of Trevice Fretum

Following the work of Tokano et al. (2014) who investigated the influence of the depth of Seldon Fretum on the tidal response of the northern seas, we study the tidal response of the Maria for three additional constant depths of Trevice Fretum: 10 m, 20 m, and 50 m which will be referred to as *Trevice A*, *Trevice B*, and *Trevice C* (the maximum depth in the reference case was 15 m). Indeed, Tokano et al. (2014) established that modifying the depth of Seldon Fretum results in phase lag (up to  $90^\circ$ ), modifications of the flow in the strait and sea surface elevation, displacement of

the amphidromic point observed in Kraken 1, and variations of the liquid exchanges between both basins of Kraken Mare.

As shown in Table 3, for  $H = 10$  m, there is no significant magnitude variation in sea surface elevation (and, hence, in tidal range) and fluid velocity with respect to the reference case except in Trevice Fretum where the maximum speed decreases by 0.033 m/s. The maximum sea surface elevation and tidal range remain located in the south-eastern part of Kraken 2 and occur at the same time (see Fig. 15). The main variation is a small displacement of the amphidromic point in Kraken 1 (it moves north-westward by about 103 km), which does not impact significantly the shape of the corange lines.

For  $H = 20$  m and  $H = 50$  m, there are much more variations with respect to the reference case. First, although the sea surface elevation remains high in the south-eastern part of Kraken 2 (about 0.136 m for *Trevice B* and 0.151 m for *Trevice C*) at the same time, this is no longer the maximum. Indeed,  $\eta$  is maximum in the eastern part of Ligeia Mare respectively 0.02 TD and 0.16 TD before perikron. As a consequence, the maximum tidal range also occurs in the eastern part of Ligeia Mare, at the location where the local maximum in Ligeia Mare was previously reached, and there are significant modifications of the tidal phase (see Fig. 16(a) and (b)). These modifications mainly occur in Kraken 1 and Ligeia Mare. Indeed, in Kraken 2, there is a small lag in the tidal phase (about  $6^\circ - 7^\circ$ ) and the tidal range at a given point change by less than 0.01 m. In contrast, in Kraken 1, modifications of  $H$  involve a large displacement of the amphidromic point north-westwards: this point moves by 430 km with respect to the benchmark for  $H = 20$  m (it is located in the south-western region of Kraken 1) and, for  $H = 50$  m, there is no amphidromic point in Kraken 1 (the shape of the lines of constant tidal phase seems to imply that it would be located somewhere on the land, south of Mayda Insula). For *Trevice C*, the tidal phase pattern suggests that, to a large extent, the tidal motion in each basin can be represented by a sloshing wave mode. Indeed, the tidal phase is nearly uniform over large geographical areas while there are strong variations (sometimes by about  $180^\circ$ ) over the straits connecting those basins (see Fig. 16(b)). The amphidromic point displacement explains the modifications of tidal range and phase observed in Kraken 1, i.e. the tidal range decreases on the northern shore and increases on the southern shore of the basin. In Ligeia Mare, increasing the depth of Trevice Fretum results in a larger tidal range. For *Trevice C*, the tidal range in Ligeia Mare is larger than everywhere else in Kraken Mare. This observation holds for *Trevice B* except for the south-eastern part of Kraken 2 (where the tidal range is maximum in the benchmark). In Trevice Fretum, the transition is different for  $H = 20$  m: the tidal range is smaller in the strait than at both outlets. This phenomenon is not observed with *Trevice A* and *C*. The other main difference in this strait occurs for  $H = 50$  m. Indeed, for such a depth, the tidal phase in Kraken 1 and Ligeia Mare are continuous. It means that the tidal motion in Ligeia Mare is no longer independent from that in Kraken 1. Indeed, for the benchmark, *Trevice A*, and *Trevice B*, the tidal phase in Ligeia Mare respectively are about  $-70^\circ$ ,  $-52^\circ$ , and  $-5^\circ$  which is significantly smaller than the tidal phase in the northern part of Kraken 1 (about  $100^\circ$ ,  $100^\circ$  and  $115^\circ$ ) while, for  $H = 50$  m, the tidal phase in Ligeia Mare is about  $75^\circ$  and increase towards Kraken 1 (but there is no transition observed in Trevice Fretum). The fact that the tides in Ligeia Mare and Kraken 1 are no longer independent can also be observed by looking at the sea surface elevation (see the video entitled "[Northern\\_seas\\_sse\\_50m](#)" in the additional content): for the reference case and *Trevice A* and *B*, there is a significant elevation gradient in both Seldon and Trevice Fretum while such a gradient is only observed in Seldon Fretum for *Trevice C*.

The depth of Trevice Fretum has a small influence on the fluid velocity out of the straits. Indeed, although some local variations

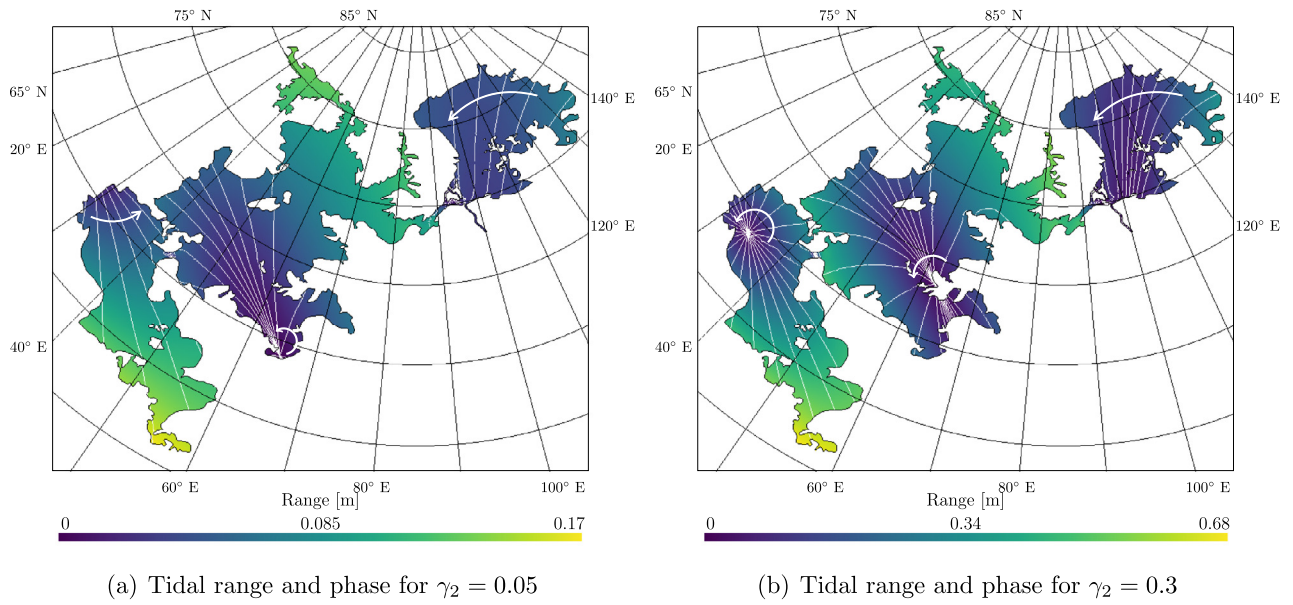


**Fig. 12.** Tidal range (in m) and tidal phase (white lines, with a 15° spacing) in Kraken and Ligeia Maria for  $\gamma_2 = 0.05$  (a) and  $\gamma_2 = 0.3$  (b). The white arrows show the direction of the tide. The maximum tidal range remains located in the south-eastern part of Kraken 2 but increases with respect to  $\gamma_2$ . The displacement of the amphidromic point in Kraken 1 is noticeable likewise the one which appears in Kraken 2. It results in an increase of the tidal range on the southern shore of Kraken 1.

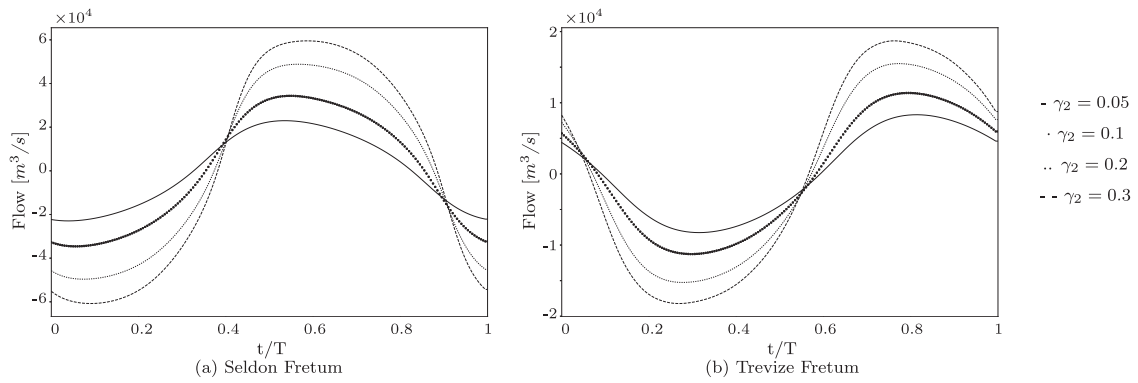


**Fig. 13.** Volumetric flow rate through Seldon (a) and Trevice Fretum (b) over one Titan day for  $\gamma_2$  ranging from 0.05 to 0.3. In Seldon and Trevice Fretum, it is respectively positive towards Kraken 1 and Ligeia Mare. In each strait, the volumetric flow rate increases with  $\gamma_2$  and a small time lag appears.

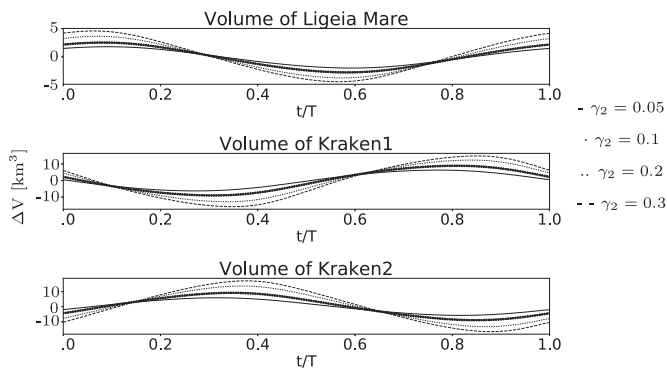


**Fig. 14.** Variation of volume in both basins of Kraken Mare and Ligeia Mare over one Titan day. In each basin, a time lag appears and the maximum volume variation rises when  $\gamma_2$  increases.

in current orientation can be observed, the global patterns remain the same (not shown). The speed increases offshore in Ligeia Mare for *Trevize B* and *C*, which is consistent with the sea surface eleva-

tion. The latter being doubled, the liquid transport is more significant and the same applies to the fluid speed. In Trevice Fretum, the speed exceeds that of the reference one only for *Trevize B* (see Table 3).

The modification of Trevice Fretum depth logically results in variations of liquid exchanges between the basins. In Seldon Fretum, there is almost no variation for *Trevize A* while for the *Trevize B* and *C*, a time lag of about 0.06 TD appears and the maximum volumetric flow rate respectively decreases and increases by 5.5% and 21.3% for *Trevize B* and *C* (see Fig. 17). The impact on the volume variation of Kraken 2 is similar: almost no variation for  $H = 10$  m and a time lag and a decrease/increase of maximum volume variation for  $H = 20, 50$  m of respectively 4.7% and 22.4%. As expected, modifying the depth of Trevice Fretum has a significant influence on the flow crossing this strait. A significant increase of the volumetric flow rate and a time lag can be observed for all implemented depths of Trevice Fretum. The maximum volumetric flow rate respectively represents 154%, 420%, and 605% of the volumetric flow rate going through Trevice Fretum in the reference case for *Trevize A, B* and *C*. The maximum volumetric flow rate is not a linear function of the depth. This implies that the liquid exchanges between the basins would be constant if the strait was

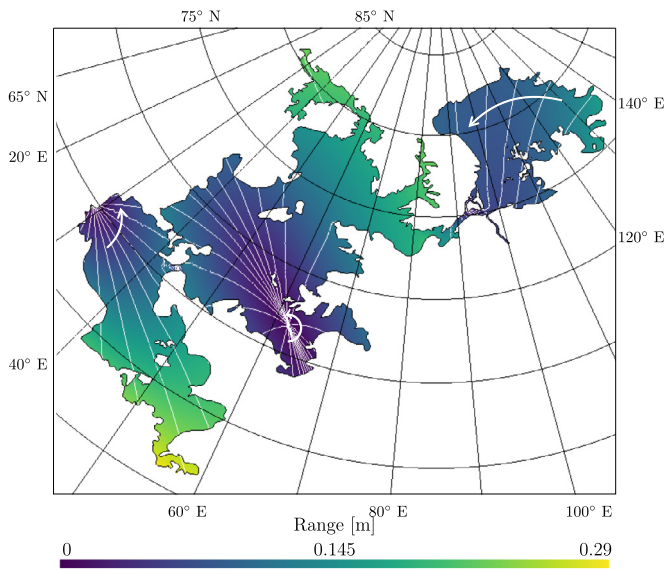


**Fig. 15.** Tidal range (in m) and tidal phase (white lines, with a  $15^\circ$  spacing) in Kraken and Ligeia Maria for  $H = 10$  m. The white arrows show the direction of the tide. The tide rotates anticlockwise and the amphidromic point in Kraken 1 moved with respect to its location for the reference case. The location and value of the maximum tidal range do not change significantly with respect to the reference case.

deeper than a certain limit (which is larger than 50 m). This result was also observed in Seldon Fretum by Tokano et al. (2014). Despite the fact that the volumetric flow rate crossing Trevize Fretum increases with the depth of the strait, this is not the case for the maximum volume variation of Kraken 1. Indeed, the latter slightly decreases when the depth increases and is smaller than the reference case for each *Trevize*. For *Trevize A*, *B*, and *C*, the volume variation in Kraken 1 represent about 97%, 93%, and 86% of  $\Delta V$  for the reference case (see Table 3). As shown in Fig. 18, the major impact of  $H$  on volume variation in Kraken 1 results in a time lag (much more significant than that observed for the volumetric flow rate in Trevize Fretum). The latter increases with the depth of

the strait and can reach up to about  $0.55 TD$ . A significant time lag is also observed in Ligeia Mare. It is the only basin of the Maria where the volume variation significantly increases with  $H$ :  $\Delta V$  increases respectively by a factor 1.57, 4.28 and 6.24 with respect to the reference case for *Trevize A*, *B* and *C*.

The time lag and modifications of volume variation resulting from the various depths also cause change in the period of time during which the sea surface elevation is positive or negative over a whole basin. There are some changes in Kraken 2: the period of time can last slightly longer (at most  $0.135 TD$ ) and a small time lag can be observed (at most  $0.055 TD$ ) but they remain minor in comparison to the variations in Ligeia Mare. Indeed, in this Mare, the period of time during which the elevation is positive (negative) over the whole domain lasts longer and longer when  $H$  rises: in contrast to the reference case, these two periods of time combined last longer than half a Titan day for *Trevize A*, *B*, and *C* (respectively  $0.535$ ,  $0.83$  and  $0.9 TD$ ). For *Trevize A* and *Trevize B* the period of time ends  $0.02 TD$  later than for the reference case and start earlier (respectively  $0.045$  and  $0.19 TD$ ) while, for *Trevize C*, the period of time starts and ends earlier (respectively  $0.395$  and about  $0.19 TD$ ).

### 4.3. Influence of the bottom friction

We study the influence of the bottom friction on the tidal response in Ligeia and Kraken Maria by varying Manning's roughness coefficient,  $n$ . The values studied range from  $0.01$  to  $0.06 \text{ sm}^{-1/3}$ , which correspond to artificial and natural bottom with stones on Earth respectively. As it can be seen in Table 3, the flow slows down as Manning's coefficient rises. A time lag also occurs: for  $n \geq 0.03 \text{ sm}^{-1/3}$  the maximum speed in Trevize and Seldon Fretum are respectively reached earlier and later than for the reference case while there is no global behaviour for  $n \leq 0.02 \text{ sm}^{-1/3}$ . As the volumetric flow rate decreases through Seldon and Trevize Fretum, the same also applies to the volume variation of each basin. As was seen before, the latter has a significant impact on the position of the amphidromic point and can modify the sea surface elevation accordingly. For instance, for  $n = 0.04 \text{ sm}^{-1/3}$ , there is an amphidromic point both in Kraken 1 and 2 while for  $n = 0.01 \text{ sm}^{-1/3}$ ,

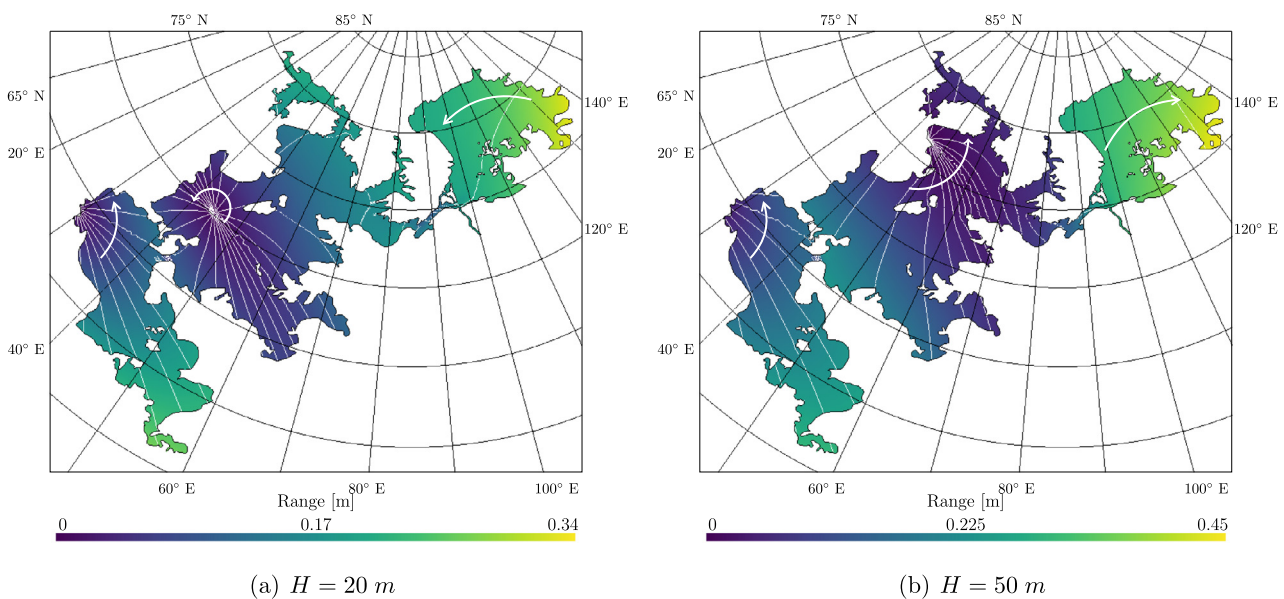


**Fig. 16.** Tidal range (in m) and tidal phase (white lines, with a  $15^\circ$  spacing) in Kraken and Ligeia Maria for  $H = 20$  m (a) and  $H = 50$  m (b). The white arrows show the direction of the tide. For  $H = 20$  m, there is a significant displacement (about 425 km) of the amphidromic point: it is now located near the western shoreline of Kraken 1 ( $70.06^\circ \text{N}$ ,  $44.49^\circ \text{E}$ ). For  $H = 50$  m, there is no amphidromic point in any basin of the Maria and no tidal phase transition through Trevize Fretum. In both case, the tidal range is now maximum in the eastern part of Ligeia Mare although it remains high in the south-eastern part of Kraken 2.

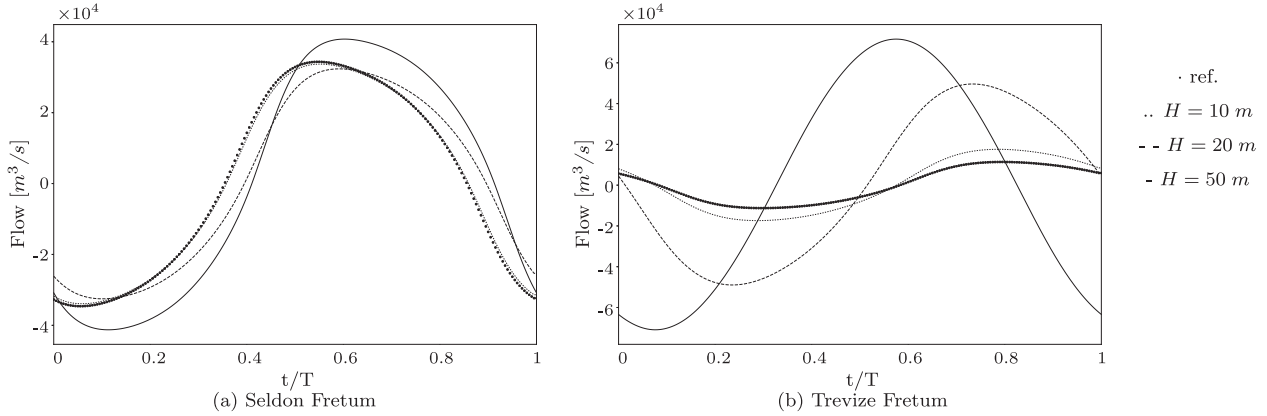


**Fig. 17.** Volumetric flow rate through Seldon (a) and Trevize Fretum (b) over one Titan day for the reference case and the three depths implemented. In Seldon and Trevize Fretum, it is respectively positive towards Kraken 1 and Ligeia Mare. The volumetric flow rate in Seldon Fretum is less sensitive to this parameter than that in Trevize but it still increases and is lagged when  $H$  varies. The volumetric flow rate in Trevize Fretum increases with  $H$  and a time lag appears.

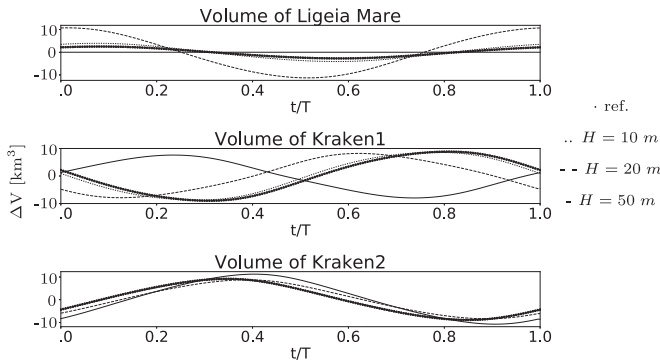


**Fig. 18.** Variation of volume in the basins of Kraken and Ligeia Maria over one Titan day. The impact of  $H$  on the volume variation is weak in Kraken 2 while it results mostly in time lag in Kraken 1. In Ligeia, the maximum volume variation increases by a factor of about 6 between  $H = 50$  m and the reference case.

there is no amphidromic point (see Table 4). Modifying  $n$  thereby results in changes of the tidal range and phase almost everywhere in the Maria: the tidal range decreases as  $n$  increases and, in Kraken Mare, it can locally change due to the displacement of the amphidromic point. Nevertheless, the maximum remains located at the same place and occurs at the same time.

#### 4.4. Influence of the artificial bathymetry

As explained in Section 2.3, a bathymetry map of Ligeia Mare is available in the literature (see Fig. 9a of Hayes (2016)). We hereby discuss to what extent an artificial bathymetry is justifiable by comparing our results obtained for the reference case to those predicted by our model when a bathymetry mimicking the bathymetry map shown in Fig. 9a of Hayes (2016) is implemented. Although the maximum depth is of the same order of magnitude for both bathymetries, there is a feature similar to a seamount near  $80^\circ\text{N}$  and Ligeia Mare is much deeper near the shore according to the bathymetry map of Hayes (2016), resulting in a higher total volume of the sea. Increasing the total volume of Ligeia Mare results in a significant modification of the liquid exchanges with Kraken Mare: the daily flow crossing Trevize is doubled. This results in almost no variation in Kraken 2: the maximum tidal range is increased by  $8\text{ mm}$ , there is small phase shift in the western part of the basin, and the maximum volume variation slightly decreases. In Kraken 1, the maximum volume variation decreases by

22% and it occurs sooner in the tidal period. As seen previously, such modifications result in a displacement of the amphidromic point. The latter is now located 233 km westward of its location in the reference case. In Ligeia Mare, there is a significant increase of the maximum tidal range (7 cm) and maximum volume variation (it is doubled) but the tidal motion remains similar. The velocity orientation can vary locally but its magnitude is globally smaller, except in Trevize Fretum where it increases.

Modifying the bathymetry of Ligeia Mare (and, hence, increasing its total volume) results in variations with respect to our reference case, the main one being a significant modification of the flow through Trevize Fretum and, hence, of the volume variation in Ligeia Mare and Kraken 1. Regarding the tidal motion, the main modification is the shift of the amphidromic point in Kraken 1. Nevertheless, the global tidal motion remains similar to that of the reference case: the tidal motions remain independent of each other in each basin and the main flow keeps its global orientation. Consequently, we consider the artificial bathymetry as justifiable for the simulation of Titan's northern seas as part of a sensitivity study.

#### 4.5. Influence of the bathymetry scaling factor

Due to the uncertainties in the bathymetry, we also conducted a study of the influence of Kraken Mare overall depth. To this end, we created two additional bathymetries *bathy A* and *bathy B* (see Section 2.4).

As expected, modifying the total volume of Kraken Mare results in modifications of the volume variation and, hence, the flow through Seldon and Trevize Fretum and the tidal phase. Diminishing/increasing the overall depth of Kraken Mare results in a reduction/rise of the tidal range, volume variation and daily flow rate through the straits. These effects are more significant in Kraken 1 and 2 and in Seldon Fretum than in Ligeia Mare and Trevize Fretum (see, for instance, the values in Table 3). For instance, with *bathy B*, the tidal range decreases by 9 cm at its maximum while it decreases by less than 2 cm in Ligeia Mare. As pointed out previously, modifications of the volume variation result in significant modifications of the tidal phase in the basins. For *bathy A*, it results in a shift of the amphidromic point of 334 km westward while the pattern of the tidal phase remains similar in Kraken 2 and Ligeia Mare although the value of the tidal phase at a given location varies (see Fig. 19(a)). For instance, the maximum sea surface elevation occurs 0.055 TD later than in the reference case. For *bathy B* on the other hand, the amphidromic point

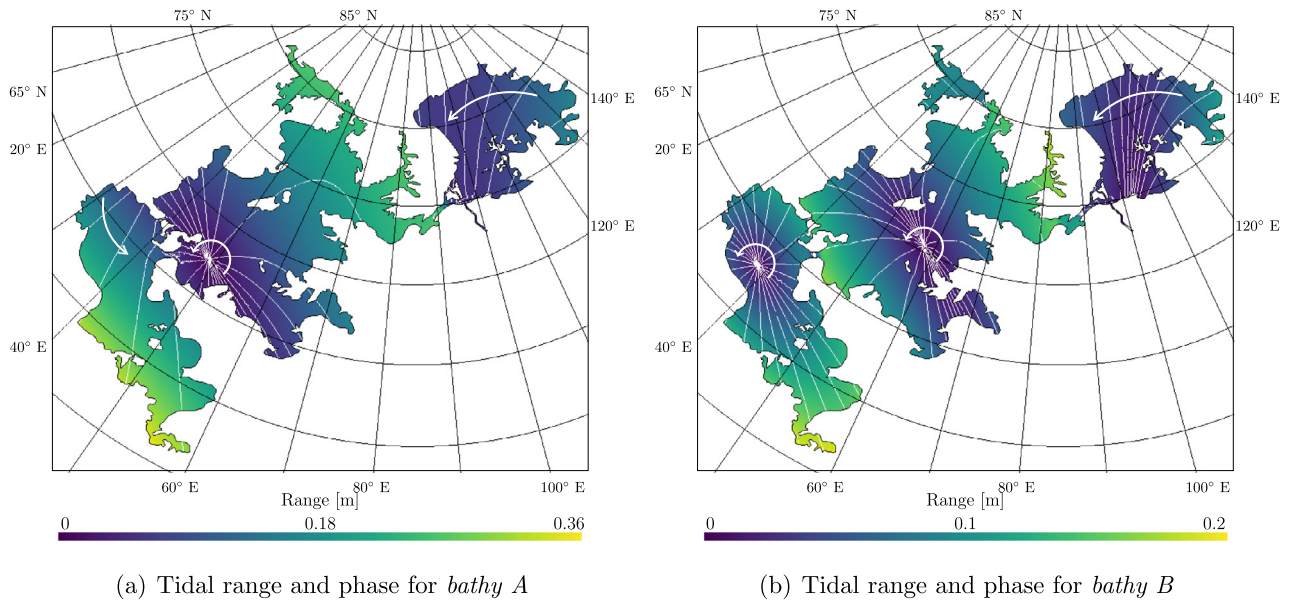


**Fig. 19.** Tidal range (in m) and tidal phase (white lines, with a 15° spacing) in Kraken and Ligeia Maria for *bathy A* (a) and *bathy B* (b). The white arrows show the direction of the tide. The maximum tidal range remains located in the south-eastern part of Kraken 2. The displacement of the amphidromic point in Kraken 1 is noticeable likewise the one which appears in Kraken 2.

shifts by 271 km north-westward in Kraken 1 and a second amphidromic point appears in Kraken 2 (see Fig. 19(b)) which results, among other things in a maximum sea surface elevation occurring 0.075  $TD$  sooner than in the reference case.

Using *bathy A* or *bathy B* can also result in local variations of the flow orientation (although the global patterns remain similar) and magnitude: the maxima remain located in the straits but they occur at different moments of the day. For instance, in Trevize Fretum, the maximum speed respectively increases/decreases for *bathy A/bathy B*.

Those results allow us to conclude that modifying significantly the total volume of Kraken Mare has a significant effect on the liquid exchanges between the basins and, hence, on their volume variation and tidal phase but the tidal motions remain independent of each other in each basin and the main flow keeps its global orientation.

## 5. Discussion

### 5.1. Influence of the model parameters

Due to uncertainties about the specific environment of Titan, various parameters of the model are poorly constrained. Some of them such as the mean density are not considered here (Vincent et al. (2016) showed that their influence is not significant on the tides) while others such as the attenuation factor and the roughness coefficient for bottom friction are discussed in this section. In addition to these parameters, the influence of the depth of Trevize Fretum and the overall bathymetry of Kraken Mare, which are unknown to this day, are also discussed.

The depth of Trevize Fretum has a significant impact on the tidal response of the Maria. Indeed, modifying the depth of this strait results in variations of the sea surface elevation, fluid velocity, and tidal phase and range in both Ligeia Mare and Kraken Mare. The results obtained with the four depths (three constant depths and the reference case) show that the volume variation of Kraken 2, Ligeia Mare, and, to a lesser extent, Kraken 1 significantly varies with the depth of Trevize Fretum. Tokano et al. (2014) reached similar conclusions about the depth of Seldon Fretum: it significantly impacts the volume variation of

both basins of Kraken Mare. They also observed the same induced variations: displacement of the amphidromic point(s), local modifications of the sea surface elevation, modification of the speed in the straits, and time lag up to 0.25  $TD$ .

As explained in Section 2.2, solid tides attenuate the liquid tides in the surface seas, which is taken into account in this work by means of an attenuation factor  $\gamma_2$ . The tidal range linearly varies with  $\gamma_2$  while the fluid velocity in the straits behaves as a semi parabola with respect to  $\gamma_2$  (see Fig. 11). Changing  $\gamma_2$  also results in displacement of amphidromic point(s) in both basins of Kraken Mare (but not in Ligeia Mare). Nevertheless, this seems to be a phenomenon induced by another effect: when  $\gamma_2$  increases, the volumetric flow rate through Seldon and Trevize Fretum and the volume variation in each basin also rise, which influences the location of the amphidromic point(s) and the tidal phase and range.

The bathymetry of Kraken Mare mostly impacts the tidal motion in Kraken Mare but it also slightly impacts that in Ligeia Mare. Multiplying the scaling factor used to compute the bathymetry (see Section 2.3) by a factor 2 results in displacement and appearance of amphidromic points in both Kraken Mare basins, which can be related to the significant variation of the flow rate in the straits linking the basins. The tidal range, maximum volume variation and flow through the strait increase with the scaling factor.

The influence of the bottom friction is related to the value of Manning's coefficient: for  $n \geq 0.03 \text{ sm}^{-1/3}$ , the fluid velocity decreases as  $n$  increases while for smaller values, no clear pattern can be observed. The consequences of this modification are mostly significant in the straits such as Trevize and Seldon Fretum: it results in variations of the liquid exchanges between the basins of the Maria. As seen previously, such variations induce significant displacement of amphidromic point(s) (leading to the appearance/disappearance of such points) and local modifications of the sea surface elevation and tidal range. For instance, the maximum sea surface elevation decreases by 0.035 m between  $n = 0.03 \text{ sm}^{-1/3}$  and  $n = 0.06 \text{ sm}^{-1/3}$  (see Table 3).

Consequently, in order to accurately predict the tides of the northern seas, one would need an accurate knowledge of the straits linking the seas: the depth and the roughness of the bottom both have a significant impact on the liquid exchanges between the

basin and, therefore, on the tides of the northern seas. The internal structure of Titan and rheology properties of the layers need also to be accurately known in order to predict as accurately as possible the value of  $\gamma_2$ . An accurate bathymetry is not needed to predict the global picture but is necessary to predict the local flow velocity and the local flow patterns. Depending on the goal of the study, an artificial bathymetry similar to the one used in this article is justifiable. Nevertheless, such an artificial bathymetry could be improved if a nearshore bathymetry similar to that derived by Hayes et al. (2010) in Ontario Lacus was available. Indeed, previous results show that, at least in Ontario Lacus, the tidal response computed with such a bathymetry was close to the tidal response predicted with a bathymetry derived from the SAR data (see Vincent et al., 2016).

### 5.2. Density variation between the basins

Although the value of the mean density does not significantly impact the model results, spatial or temporal variations of the density would result in significant additional forcing due to the resulting density gradient. Local variations could be induced by meteorological events such as precipitation and evaporation or due to the vertical profile of the absorption of sunlight. Such phenomena were previously studied by Tokano and Lorenz (2016). According to their results, the flow in the straits linking the basins of the northern seas is weaker (by about one order of magnitude) than that induced by the tides while it can be larger in the middle of the basins depending on the light extinction coefficient. There could also be a liquid composition difference between Ligeia Mare and Kraken Mare due to surface temperature variation with the latitude (Lorenz, 2014). Such a liquid composition variation between Kraken Mare and Ligeia Mare, if exists, would result in significant density gradient and imply that the tidal mixing between Ligeia Mare and Kraken Mare is too weak to overcome the precipitation/evaporation forcing difference between those seas. The gradient would significantly modify the flow in Trevize Fretum and, hence, the liquid exchanges between Ligeia Mare and Kraken Mare. Such density counterflows are also encountered on Earth (e.g. in the Strait of Gibraltar). Nevertheless, the tides can be studied apart from this phenomenon as it does not modify the tidal forcing nor the parameters of this model.

### 5.3. Shoreline

We implemented the shoreline from Radar images. Nevertheless, the whole shoreline is not mapped in high resolution which makes it difficult to accurately draw it. Moreover, the Radar interprets some shallow areas as dry ground. This results in uncertain shorelines. For instance, our implementation differs from Tokano et al. (2014) in various respects:

- Trevize Fretum is implemented as an elongated (200 km) narrow (15 km) strait with small channels near Ligeia outlet instead of a set of short (150 km) and narrow (20 km) straits.
- The link between both basins of Kraken Mare next to Seldon Fretum is represented by two narrow channels instead of a wide connexion with two small islands.
- We took into account some islands ignored by Tokano et al. (2014): in the southern part of Ligeia Mare, the middle of Kraken 2, and the east of Kraken 1 (see Fig. 1 in Tokano et al. (2014))

The interpretation of Lorenz et al. (2014) is different from both ours and Tokano's: the global shape of the shoreline and the islands of Lorenz et al. (2014) are closer to that used by Tokano et al. (2014) but our implementation of Seldon and Trevize Fretum is closer to that of Lorenz et al. (2014) than to that

of Tokano et al. (2014). Such variations of the shoreline are doubly important because our bathymetry (as well as Tokano's) depends on the distance to the shore. Consequently, taking into account an island or ignoring it can significantly modify the bathymetry. Additionally to this effect, the shape of the seas can locally generate high speed currents (near a cape or a peninsula) and the shape (width and length) of a strait has a significant impact on the liquid exchanges between the basins. In order to enhance the quality of our predictions, a more accurate map of the northern seas shoreline would be needed. Unfortunately, this will request another mission as Cassini has now fallen into Saturn.

### 5.4. Comparison with previous results

The tidal response of Ligeia and Kraken Maria has already been studied by means of numerical simulation by Tokano (2010) and Tokano et al. (2014). In this section, we compare our results obtained for the reference case with the predictions of Tokano et al. (2014). First of all, we will list the discrepancies between our model and that used by Tokano et al. (2014). Then, we will compare our results.

In terms of model design, the main difference is that Tokano et al. (2014) used a 3D baroclinic ocean circulation model while we used a 2D barotropic shallow water model. Nevertheless, although Tokano's model is better suited to study complex interactions, it is usually not necessary to have recourse to a 3D model to predict the tidal response of a sea. There are also some minor discrepancies in the shoreline of the Maria which results in local variations of the bathymetry. For instance, in Seldon Fretum, the depth scales with the distance to the shore and the maximum is about 16 m while Tokano et al. (2014) implemented a constant depth of 12 m and the shape of the straits slightly varies (see Section 5.3). Despite these discrepancies, the main parameters are similar: the same forcing is applied,  $\gamma_2 = 0.1$ , and the depth scales with the distance to the shore.

In both simulations, the tide propagates in the same direction (i.e. anticlockwise in Kraken 1, westwards in Ligeia Mare between perikron and perikron + 0.25 TD, ...), there is a sharp transition in sea surface elevation in the strait linking both basins of Kraken Mare ( $\eta$  is positive at one outlet and negative at the other at perikron and 0.25 TD later), and an amphidromic point is observed in Kraken 1 in the same area (the small variation of position could be due to the modification of volume variation in this basin (it has a significant influence on the position of such a point, see Section 4.2)). The tidal range predicted in each Mare is maximum at the same location as in Tokano et al. (2014) although it is slightly smaller (0.29 m instead of 0.37 m) in Kraken Mare and slightly larger (0.14 m instead of 0.1 m) in Ligeia Mare. This could be due to the difference in the shape of the small channels near Seldon Fretum (Tokano et al. (2014) implemented it as a wider connection, resulting in larger liquid exchanges between both basins of Kraken Mare) and Trevize Fretum. This can be seen by comparing the maximum volume variation of each basin: almost the same magnitude is predicted in Ligeia Mare (2.5 km<sup>3</sup> versus about 2 km<sup>3</sup> for Tokano et al. (2014)) while we predicted a smaller one in both basins of Kraken Mare (this could be due to the fact that the bathymetry of Seldon Fretum is significantly different). The sea surface elevation at perikron and 0.25 TD after perikron are close to those predicted by Tokano et al. (2014) but there are also some differences:  $\eta$  is high/low at the same locations but the magnitude can vary locally. For instance, the elevation predicted by our model at perikron is smaller in the southeastern part of Kraken 2 and can be slightly larger in the eastern part of Ligeia Mare. The tidal currents predicted by both models are also similar: it is small offshore and maximum in the strait where it can reach 0.36 m/s and 0.14 m/s according to our model

and to Tokano et al. (2014) (for a depth of 12 m). The difference in Seldon Fretum strait between the implementations could explain such variations. In the straits, the velocity is directed towards the area where  $\eta$  is the smaller. In conclusion, our results are close to those of Tokano et al. (2014). Although some discrepancies occur, they can be linked to the differences between the models, particularly to the variations in the shape and depth of the two main straits, Trevice and Seldon Fretum. Both models have their advantages, that of SLIM being the higher resolution used to represent the shoreline, the wide range of parameters values studied, and the use of tracers to study the liquid exchanges.

## 6. Applications and future missions

As discussed previously, there are a few parameters which remain poorly constrained. One way of improving our model is to get additional data in order to constrain these parameters. Unfortunately, Cassini reached the end of its life and fell into Saturn during its “Grand finale”. Consequently, providing further data about Titan requests to plan further mission(s). So far, various proposals have been discussed: a drifted capsule (TiME, see Lorenz et al., 2012), an orbiter and a lake probe (E2T, see Mitri et al., 2014), a submarine (Titan sub, see Hartwig et al., 2016), and an orbiter (Oceanus, see Sotin et al., 2017). Among these missions, several (Lorenz et al., 2012; Mitri et al., 2014; Hartwig et al., 2016) plan to send a vehicle in the northern seas. In order to organise such missions, various above-mentioned results are of high interest: the tidal range is of interest in knowing whether a floating capsule like the Titan Mare Explorer (or related European proposals) could be grounded and refloated from the beach or a tidal flat over a tidal cycle; a particle tracking model can predict the position of a capsule as a function of time and landing time and position; the tidal flow is of interest in order to size the propulsion system of a boat/submarine that should overcome the current in Trevice/Seldon Fretum or to assess over what fraction of the tidal cycle a submarine could or could not sail through the straits.

These missions could improve significantly our knowledge of Titan. Among the observations/data that could be provided, some of them would be useful for our model:

- An orbiter could detect the tides of the surface seas with a precision altimeter and provide a map of the sea surface elevation as a function of time. Such observations on Earth have been able to constrain internal processes in the oceans such as the tidal dissipation (e.g. Egbert and Ray, 2000).
- An orbiter could provide images in the visual band of the surface lakes and seas. Such images could be used to predict the surface flow of the sea (see, e.g. Delandmeter et al., 2017) by means of Particle Image Velocimetry (Chen, 2011) or by Global Optimal Solution (Tseng et al., 2012).
- An orbiter could isolate the crustal response to constrain  $\gamma_2$  by means of altimetry/gravimetry.
- A sounder could constrain the bathymetry of the northern seas (presently details on Kraken are particularly lacking) with a high resolution. If we pay interest to the global behaviour, a structured grid of 2–3 km resolution would be enough but a higher resolution would be needed in Seldon and Trevice Fretum and in specific areas such as Moray Sinus or at the Magic Islands emplacements. To this end, there are at least two relevant kinds of sounder:
  - A radar system, operating from orbit (or from an aerial platform) could possibly detect a discontinuity in dielectric constant.
  - An acoustic sounder (depth sounder/sonar) on a vehicle on/in the sea would detect a discontinuity in acoustic impedance (e.g. Arvelo and Lorenz, 2013).

A sharp change in composition or temperature could yield detectable reflections to either type of instrument, but in each case the reflection at such a liquid–liquid interface would likely not be so severe as to suppress the echo from the much stronger dielectric/acoustic contrast between liquid and the solid seabed.

- A lander with a view of the shoreline could constrain the tidal motion at some specific locations allowing for time series of sea surface elevation and velocity at these points.
- A submarine or a floating capsule could constrain the liquid composition and the stratification of the surface seas and study the tidal current.

Such data/observations could be used to constrain the value of the parameters. Furthermore, it would provide data that could be used as input(s) for other model(s) and to study accurately local phenomena. For instance, providing the flow velocity, sea surface elevation, temperature and composition along a line joining the shore of Ligeia (Kraken) Mare away from the outlet/inlet of the strait would allow one to study Trevice Fretum accurately (i.e. with a high resolution mesh) by means of a 3D oceanographic model.

## 7. Conclusion

Hydrocarbon filled liquid bodies have been known to exist on Titan’s surface since Cassini radar observations from 2006 (Stofan et al., 2007). In this paper we studied the tidal response of the two largest seas, namely Kraken Mare and Ligeia Mare, which are linked by a strait called Trevice Fretum. To do so, we used SLIM (<http://www.climate.be/slim>), a model previously adapted to Titan conditions (Vincent et al., 2016). A sensitivity analysis with respect to various poorly constrained parameters such as the bottom friction, the depth of Trevice Fretum, the overall depth of Kraken Mare, and the attenuation factor due to the sea bottom tidal deformations was conducted. This study brings further insight in the liquid exchanges between the basins and the influence of these parameters on the tidal response of the northern seas.

Our model predicts an independent tide, with an exact period of 1 *TD* (Titan Day), in each basin of Kraken Mare and Ligeia Mare. In the northern basin of Kraken Mare, the tide rotates anticlockwise around an amphidromic point located in its south-eastern part. The tidal phase suggests that, to a large extent, the tidal motion in Kraken 1 and Ligeia Mare can be represented by a sloshing wave mode. Indeed, in these basins, the tidal phase is nearly uniform over large geographical areas while there are strong variations over the straits connecting those basins with Kraken 1. The maximum tidal range (about 0.29 m) is located in the south-eastern part of the southern basin of Kraken Mare and occurs 0.31 *TD* after perikron (high tide)/apokron (low tide). The fluid speed is one order of magnitude larger in Trevice and Seldon Fretum than offshore in Kraken or Ligeia Mare. The maximum in each strait respectively is 0.24 and 0.36 m/s. No resonance phenomenon was observed in the northern seas. Some of the seas eigenmodes correspond to coastal trapped waves or to funnel shaped resonance but their periods are much smaller than the tidal period. The maximum volume variation in both basins of Kraken Mare are about three times larger (respectively 8.9 km<sup>3</sup> for the northern one and 9.2 km<sup>3</sup> for the southern one) than that of Ligeia Mare (about 2.5 km<sup>3</sup>). These results are overall rather similar to those of Tokano et al. (2014), suggesting that a 2D model is adequate for modelling many aspects of Titan’s tides and may be better for parametric studies since it is less computationally demanding than a 3D model.

We studied the influence of Trevize Fretum depth, of the bathymetry scaling factor  $\alpha$ , of the attenuation factor  $\gamma_2$  and of the bottom friction. They have a significant influence on the tidal response of each basin, mainly by modifying the liquid exchanges between the basins. Indeed, modifying the depth of Trevize Fretum logically leads to changes of the liquid exchanges through the strait. The bottom friction has an impact on the speed: as the bottom friction increases, the speed decreases (and consequently the liquid exchanges through the straits). Increasing  $\gamma_2$  (and thereby the forcing) results in larger liquid exchanges. The bathymetry scaling factor modifies the volume ratio between Kraken Mare and Ligeia Mare as well as the total amount of liquid in Kraken Mare which, in turns, modifies the liquid exchanges. Such variations lead to the displacement of amphidromic point(s) in both basins of Kraken Mare, significant time lag, and can modify the location at which the tidal range is maximum.

### Acknowledgements

Computational resources were provided by the Consortium des Équipements de Calcul Intensif (CÉCI), funded by the Belgian Fund for Scientific Research (F.R.S.-FNRS) under Grant No. 2.5020.11. Eric Deleersnijder is an honorary Research associate with the F.R.S.-FNRS, Özgür Karatekin is funded by the Belgian PRODEX, managed by the ESA, in collaboration with the Belgian Federal Science Policy Office. Ralph Lorenz acknowledges the support of NASA Outer Planets Research grant NNX13AK97G.

We would like to thank the Cassini Radar team and the SLIM team for their help.

### Supplementary Materials

Supplementary material associated with this article can be found, in the online version, at [10.1016/j.icarus.2017.12.018](https://doi.org/10.1016/j.icarus.2017.12.018).

### References

- Aharonson, O., Hayes, A.G., Lunine, J.I., Lorenz, R.D., Allison, M.D., Elachi, C., 2009. An asymmetric distribution of lakes on Titan as a possible consequence of orbital forcing. *Nat. Geosci.* 2 (12), 851–854. doi:[10.1038/ngeo698](https://doi.org/10.1038/ngeo698).
- Anderson, E.J., Schwab, D.J., 2013. Predicting the oscillating bi-directional exchange flow in the straits of Mackinac. *J. Great Lakes Res.* 39 (4), 663–671. doi:[10.1016/j.jglr.2013.09.001](https://doi.org/10.1016/j.jglr.2013.09.001).
- Arvelo, J., Lorenz, R.D., 2013. Plumbing the depths of Ligeia: considerations for depth sounding in Titan's hydrocarbon seas. *J. Acoust. Soc. Am.* 134 (6), 4335–4350. doi:[10.1121/1.4824908](https://doi.org/10.1121/1.4824908).
- Atreya, S.K., Adams, E.Y., Niemann, H.B., Demick-Montelara, J.E., Owen, T.C., Fulchignoni, M., Ferri, F., Wilson, E.H., 2006. Titan's methane cycle. *Planet. Space Sci.* 54 (12), 1177–1187. doi:[10.1016/j.pss.2006.05.028](https://doi.org/10.1016/j.pss.2006.05.028).
- Baland, R.-M., Tobie, G., Lefèvre, A., Van Hoolst, T., 2014. Titan's internal structure inferred from its gravity field, shape, and rotation state. *Icarus* 237, 29–41. doi:[10.1016/j.icarus.2014.04.007](https://doi.org/10.1016/j.icarus.2014.04.007).
- Baland, R.-M., Van Hoolst, T., Yseboodt, M., Karatekin, Ö., 2011. Titan's obliquity as evidence of a subsurface ocean? *Astron. Astrophys.* 530, A141. doi:[10.1051/0004-6361/201116578](https://doi.org/10.1051/0004-6361/201116578).
- Bernard, P.-E., Deleersnijder, E., Legat, V., Remacle, J.-F., 2008. Dispersion analysis of discontinuous Galerkin schemes applied to Poincaré, Kelvin and Rossby waves. *J. Sci. Comput.* 34 (1), 26–47. doi:[10.1007/s10915-007-9156-6](https://doi.org/10.1007/s10915-007-9156-6).
- Beuthe, M., 2015. Tidal Love numbers of membrane worlds: Europa, Titan, and Co. *Icarus* 57 (258), 239–266. doi:[10.1007/s10236-006-0093-y](https://doi.org/10.1007/s10236-006-0093-y).
- Brown, R.H., Soderblom, L.A., Soderblom, J.M., Clark, R.N., Jaumann, R., Barnes, J.W., Sotin, C., Buratti, B., Baines, K.H., Nicholson, P.D., 2008. The identification of liquid ethane in Titan's Ontario Lacus. *Nature* 454 (7204), 607–610. doi:[10.1038/nature07100](https://doi.org/10.1038/nature07100).
- de Brye, B., de Brauwere, A., Gourgue, O., Kärnä, T., Lambrechts, J., Comblen, R., Deleersnijder, E., 2010. A finite-element, multi-scale model of the Scheldt tributaries, river, estuary and ROFI. *Coast. Eng.* 57 (9), 850–863. doi:[10.1016/j.coastaleng.2010.04.001](https://doi.org/10.1016/j.coastaleng.2010.04.001).
- de Brye, B., Schellen, S., Sassi, M., Vermeulen, B., Kärnä, T., Deleersnijder, E., Hoitink, T., 2011. Preliminary results of a finite-element, multi-scale model of the Mahakam Delta (Indonesia). *Ocean Dyn.* 61 (8), 1107–1120. doi:[10.1007/s10236-011-0410-y](https://doi.org/10.1007/s10236-011-0410-y).
- Chen, W., 2011. Nonlinear inverse model for velocity estimation from an image sequence. *J. Geophys. Res.-Oceans* 116 (C6). doi:[10.1029/2010JC006924](https://doi.org/10.1029/2010JC006924).
- Cordier, D., Mousis, O., Lunine, J.I., Lavvas, P., Vuitton, V., 2009. An estimate of the chemical composition of Titan's lakes. *Astrophys. J. Lett.* 707 (2), L128. doi:[10.1088/0004-637X/707/2/L128](https://doi.org/10.1088/0004-637X/707/2/L128).
- Cottini, V., Nixon, C.A., Jennings, D.E., de Kok, R., Teanby, N.A., Irwin, P.G.J., Flasar, F.M., 2012. Spatial and temporal variations in Titan's surface temperatures from Cassini CIRS observations. *Planet. Space Sci.* 60 (1), 62–71. doi:[10.1016/j.pss.2011.03.015](https://doi.org/10.1016/j.pss.2011.03.015).
- Delandmeter, P., Lambrechts, J., Marmorino, G.O., Legat, V., Wolanski, E., Remacle, J.-F., Chen, W., Deleersnijder, E., 2017. Submesoscale tidal eddies in the wake of coral islands and reefs: satellite data and numerical modelling. *Ocean Dyn.* 1–17. doi:[10.1007/s10236-017-1066-z](https://doi.org/10.1007/s10236-017-1066-z).
- Dermott, S.F., Sagan, C., 1995. Tidal effects of disconnected hydrocarbon seas on Titan. *Nature* 374 (6519), 238–240. doi:[10.1038/374238a0](https://doi.org/10.1038/374238a0).
- Egbert, G.D., Ray, R.D., 2000. Significant dissipation of tidal energy in the deep ocean inferred from satellite altimeter data. *Nature* 405 (6788), 775–778. doi:[10.1038/35015531](https://doi.org/10.1038/35015531).
- Geuzaine, C., Remacle, J.-F., 2009. Gmsh: A 3-D finite element mesh generator with built-in pre- and post-processing facilities. *Int. J. Numer. Methods Eng.* 79 (11), 1309–1331. doi:[10.1002/nme.2579](https://doi.org/10.1002/nme.2579).
- Glein, C.R., Shock, E.L., 2013. A geochemical model of non-ideal solutions in the methane–ethane–propane–nitrogen–acetylene system on Titan. *Geochim. Cosmochim. Ac.* 115, 217–240. doi:[10.1016/j.gca.2013.03.030](https://doi.org/10.1016/j.gca.2013.03.030).
- Gordeev, R.G., Kagan, B.A., Polyakov, E.V., 1977. The effects of loading and self-attraction on global ocean tides: the model and the results of a numerical experiment. *J. Phys. Oceanogr.* 7 (2), 161–170. doi:[10.1175/1520-0485\(1977\)007\(0161:TEOLAS\)2.0.CO;2](https://doi.org/10.1175/1520-0485(1977)007(0161:TEOLAS)2.0.CO;2).
- Hanel, R., Conrath, B., Flasar, F.M., Kunde, V., Maguire, W., Pearl, J., Pirraglia, J., Samuelson, R., Herath, L., Allison, M., Cruikshank, D., Gautier, D., Gierasch, P., Horn, L., Koppany, R., 1981. Infrared observations of the saturnian system from Voyager-1. *Science* 212, 192–200. doi:[10.1126/science.212.4491.192](https://doi.org/10.1126/science.212.4491.192).
- Hartwig, J.W., Colozza, A., Lorenz, R.D., Oleson, S., Landis, G., Schmitz, P., Paul, M., Walsh, J., 2016. Exploring the depths of Kraken Mare—power, thermal analysis, and ballast control for the Saturn Titan submarine. *Cryogenics* 74, 31–46. doi:[10.1016/j.cryogenics.2015.09.009](https://doi.org/10.1016/j.cryogenics.2015.09.009).
- Hayes, A.G., 2016. The lakes and seas of Titan. *Annu. Rev. Earth Planet. Sci.* 44. doi:[10.1146/annurev-earth-060115-012247](https://doi.org/10.1146/annurev-earth-060115-012247).
- Hayes, A.G., Aharonson, O., Callahan, P., Elachi, C., Gim, Y., Kirk, R.L., Lewis, K., Lopes, R., Lorenz, R.D., Lunine, J.I., et al., 2008. Hydrocarbon lakes on Titan: Distribution and interaction with a porous regolith. *Geophys. Res. Lett.* 35 (9). doi:[10.1029/2008GL033409](https://doi.org/10.1029/2008GL033409).
- Hayes, A.G., Aharonson, O., Lunine, J.I., Kirk, R.L., Zebker, H.A., Wye, L.C., Lorenz, R.D., Turtle, E.P., Paillou, P., Mitri, G., et al., 2011. Transient surface liquid in Titan's polar regions from Cassini. *Icarus* 211 (1), 655–671. doi:[10.1029/2009JE003557](https://doi.org/10.1029/2009JE003557).
- Hayes, A.G., Lorenz, R.D., Donelan, M.A., Manga, M., Lunine, J.I., Schneider, T., Lamb, M.P., Mitchell, J.M., Fischer, W.W., Graves, S.D., et al., 2013. Wind driven capillary-gravity waves on Titan's lakes: hard to detect or non-existent? *Icarus* 225 (1), 403–412. doi:[10.1016/j.icarus.2013.04.004](https://doi.org/10.1016/j.icarus.2013.04.004).
- Hayes, A.G., Mastrogiuseppe, M., Lunine, J.I., Poggiali, V., Lorenz, R.D., Mitchell, K.M., Malaska, M.J., Le Gall, A., 2016. The bathymetry and composition of Titan's lakes and seas. In: *47th Lunar and Planetary Science Conference*, p. 1904.
- Hayes, A.G., Wolf, A.S., Aharonson, O., Zebker, H., Lorenz, R.D., Kirk, R.L., Paillou, P., Lunine, J.I., Wye, L., Callahan, P., et al., 2010. Bathymetry and absorptivity of Titan's Ontario Lacus. *J. Geophys. Res.-Planet* 115 (E9), E09009. doi:[10.1029/2009JE003557](https://doi.org/10.1029/2009JE003557).
- Hemingway, D., Nimmo, F., Zebker, H., Iess, L., 2013. A rigid and weathered ice shell on Titan. *Nature* 500 (7464), 550–552. doi:[10.1038/nature12400](https://doi.org/10.1038/nature12400).
- Hendershott, M.C., 1972. The effects of solid earth deformation on global ocean tides. *Geophys. J. Int.* 29 (4), 389–402. doi:[10.1111/j.1365-246X.1972.tb06167.x](https://doi.org/10.1111/j.1365-246X.1972.tb06167.x).
- Henry, R.F., Walters, R.A., 1993. Geometrically based, automatic generator for irregular triangular networks. *Commun. Numer. Methods Eng.* 9 (7), 555–566. doi:[10.1002/cnm.1640090703](https://doi.org/10.1002/cnm.1640090703).
- Hofgartner, J.D., Hayes, A.G., Lunine, J.I., Zebker, H., Lorenz, R.D., Malaska, M.J., Mastrogiuseppe, M., Notarnicola, C., Soderblom, J.M., 2016. Titans "Magic Islands": transient features in a hydrocarbon sea. *Icarus* 271, 338–349. doi:[10.1016/j.icarus.2016.02.022](https://doi.org/10.1016/j.icarus.2016.02.022).
- Hofgartner, J.D., Hayes, A.G., Lunine, J.I., Zebker, H., Stiles, B.W., Sotin, C., Barnes, J.W., Turtle, E.P., Baines, K.H., Brown, R.H., et al., 2014. Transient features in a Titan sea. *Nat. Geosci.* 7 (7), 493–496. doi:[10.1038/ngeo2190](https://doi.org/10.1038/ngeo2190).
- Iess, L., Jacobson, R.A., Ducci, M., Stevenson, D.J., Lunine, J.I., Armstrong, J.W., Asmar, S.W., Racioppa, P., Rappaport, N.J., Tortora, P., 2012. The tides of Titan. *Science* 337 (6093), 457–459. doi:[10.1126/science.1219631](https://doi.org/10.1126/science.1219631).
- Kärnä, T., De Brye, B., Gourgue, O., Lambrechts, J., Comblen, R., Legat, V., Deleersnijder, E., 2011. A fully implicit wetting-drying method for DG-FEM shallow water models, with an application to the Scheldt Estuary. *Comput. Method Appl. Mech.* 200 (5), 509–524. doi:[10.1016/j.cma.2010.07.001](https://doi.org/10.1016/j.cma.2010.07.001).
- Lambrechts, J., Hanert, E., Deleersnijder, E., Bernard, P.-E., Legat, V., Remacle, J.-F., Wolanski, E., 2008. A multi-scale model of the hydrodynamics of the whole Great Barrier Reef. *Estuar. Coast Shelf Sci.* 79 (1), 143–151. doi:[10.1016/j.ecss.2008.03.016](https://doi.org/10.1016/j.ecss.2008.03.016).
- Le Gall, A., Malaska, M.J., Lorenz, R.D., Janssen, M.A., Tokano, T., Hayes, A.G., Mastrogiuseppe, M., Lunine, J.I., Veyssière, G., Encrenaz, P., et al., 2016. Composition, seasonal change and bathymetry of Ligeia Mare, Titan, derived from its microwave thermal emission. *J. Geophys. Res.-Planet* 121 (2), 233–251. doi:[10.1002/2015JE004920](https://doi.org/10.1002/2015JE004920).

- LeBlond, P.H., Mysak, L.A., 1978. Chapter 3 free waves: long wavelengths. In: LeBlond, P.H., Mysak, L.A. (Eds.), Elsevier Oceanography Series. In: Waves in the Ocean, 20. Elsevier, pp. 119–196. doi:[10.1016/S0422-9894\(08\)70816-X](https://doi.org/10.1016/S0422-9894(08)70816-X).
- Lefevre, A., Tobie, G., Choblet, G., Čadež, O., 2014. Structure and dynamics of Titan's outer icy shell constrained from Cassini data. *Icarus* 237, 16–28. doi:[10.1016/j.icarus.2014.04.006](https://doi.org/10.1016/j.icarus.2014.04.006).
- Legrand, S., Deleersnijder, E., Hanert, E., Legat, V., Wolanski, E., 2006. High-resolution, unstructured meshes for hydrodynamic models of the Great Barrier Reef, Australia. *Estuar. Coast Shelf Sci.* 68 (1), 36–46. doi:[10.1016/j.ecss.2005.08.017](https://doi.org/10.1016/j.ecss.2005.08.017).
- Lorenz, R.D., 2014. The flushing of Ligeia: composition variations across Titan's seas in a simple hydrological model. *Geophys. Res. Lett.* 41 (16), 5764–5770. doi:[10.1002/2014GL061133](https://doi.org/10.1002/2014GL061133).
- Lorenz, R.D., Kirk, R.L., Hayes, A.G., Anderson, Y.Z., Lunine, J.I., Tokano, T., Turtle, E.P., Malaska, M.J., Soderblom, J.M., Lucas, A., et al., 2014. A radar map of Titan seas: tidal dissipation and ocean mixing through the throat of Kraken. *Icarus* 237, 9–15. doi:[10.1016/j.icarus.2014.04.005](https://doi.org/10.1016/j.icarus.2014.04.005).
- Lorenz, R.D., Tokano, T., Newman, C.E., 2012. Winds and tides of Ligeia Mare, with application to the drift of the proposed time TiME (Titan Mare Explorer) capsule. *Planet. Space Sci.* 60 (1), 72–85. doi:[10.1016/j.pss.2010.12.009](https://doi.org/10.1016/j.pss.2010.12.009).
- Luspay-Kuti, A., Chevrier, V.F., Cordier, D., Rivera-Valentin, E.G., Singh, S., Wagner, A., Wasiak, F.C., 2015. Experimental constraints on the composition and dynamics of Titan's polar lakes. *Earth Planet Sci. Lett.* 410, 75–83. doi:[10.1016/j.epsl.2014.11.023](https://doi.org/10.1016/j.epsl.2014.11.023).
- Mastroggiuseppe, M., Poggiali, V., Hayes, A.G., Lorenz, R.D., Lunine, J.I., Picardi, G., Seu, R., Flamini, E., Mitri, G., Notarnicola, C., et al., 2014. The bathymetry of a Titan sea. *Geophys. Res. Lett.* 41 (5), 1432–1437. doi:[10.1002/2013GL058618](https://doi.org/10.1002/2013GL058618).
- McEwen, A.S., Turtle, E., Perry, J., Dawson, D., Fussner, S., Collins, G., Porco, C., Johnson, T., Soderblom, L., 2005. Mapping and monitoring the surface of Titan. In: *AAS/Division for Planetary Sciences Meeting Abstracts #37*, 37, p. 739.
- Mitri, G., Coustenis, A., Fanchini, G., Hayes, A.G., Iess, L., Khurana, K., Lebreton, J.-P., Lopes, R.M., Lorenz, R.D., Meriggiola, R., et al., 2014. The exploration of Titan with an orbiter and a lake probe. *Planet. Space Sci.* 104, 78–92. doi:[10.1016/j.pss.2014.07.009](https://doi.org/10.1016/j.pss.2014.07.009).
- Nimmo, F., Bills, B.G., 2010. Shell thickness variations and the long-wavelength topography of Titan. *Icarus* 208 (2), 896–904. doi:[10.1016/j.icarus.2010.02.020](https://doi.org/10.1016/j.icarus.2010.02.020).
- Poggiali, V., Mastroggiuseppe, M., Hayes, A.G., Seu, R., Birch, S.P.D., Lorenz, R.D., Grima, C., Hofgartner, J.D., 2016. Liquid-filled canyons on Titan. *Geophys. Res. Lett.* 43 (15), 7887–7894. doi:[10.1002/2016GL069679](https://doi.org/10.1002/2016GL069679).
- Rappaport, N.J., Iess, L., Wahr, J., Lunine, J.I., Armstrong, J.W., Asmar, S.W., Tortora, P., Di Benedetto, M., Racioppa, P., 2008. Can Cassini detect a subsurface ocean in Titan from gravity measurements? *Icarus* 194 (2), 711–720. doi:[10.1016/j.icarus.2007.11.024](https://doi.org/10.1016/j.icarus.2007.11.024).
- Sagan, C., Dermott, S.F., 1982. The tide in the seas of Titan. *Nature* 300 (5894), 731–733. doi:[10.1038/300731a0](https://doi.org/10.1038/300731a0).
- Samuelson, R.E., Hanel, R.A., Kunde, V.G., Maguire, W.C., 1981. Mean molecular weight and hydrogen abundance of Titan's atmosphere. *Nature* 292, 688–693.
- Sears, W.D., 1995. Tidal dissipation in oceans on Titan. *Icarus* 113 (1), 39–56. doi:[10.1006/icar.1995.1004](https://doi.org/10.1006/icar.1995.1004).
- Smagorinsky, J., 1963. General circulation experiments with the primitive equations: I. the basic experiment. *Mon. Weather Rev.* 91 (3), 99–164. doi:[10.1175/1520-0493\(1963\)091<0099:GCEWTP>2.3.CO;2](https://doi.org/10.1175/1520-0493(1963)091<0099:GCEWTP>2.3.CO;2).
- Sohl, F., Hussmann, H., Schwentker, B., Spohn, T., Lorenz, R.D., 2003. Interior structure models and tidal Love numbers of Titan. *J. Geophys. Res.-Planet* 108 (E12). doi:[10.10029/2003JE002044](https://doi.org/10.10029/2003JE002044).
- Sohl, F., Sears, W.D., Lorenz, R.D., 1995. Tidal dissipation on Titan. *Icarus* 115 (2), 278–294. doi:[10.1006/icar.1995.1097](https://doi.org/10.1006/icar.1995.1097).
- Sohl, F., Solomonidou, A., Wagner, F.W., Coustenis, A., Hussmann, H., Schulze-Makuch, D., 2014. Structural and tidal models of Titan and inferences on cryovolcanism. *J. Geophys. Res.-Planet* 119 (5), 1013–1036. doi:[10.1002/2013JE004512](https://doi.org/10.1002/2013JE004512).
- Sotin, C., Hayes, A.G., Malaska, M.J., Nimmo, F., Trainer, M., Mastroggiuseppe, M., Soderblom, J.M., Tortora, P., Hofgartner, J.D., Aharonson, O., Barnes, J.W., Hodys, R., Iess, L., Kirk, R.L., Lavvas, P., Lorenz, R.D., Lunine, J.I., Mazarico, E., McEwen, A.S., Neish, C., Nixon, C.A., Turtle, E.P., Vuitton, V., Yelle, R., 2017. Oceanus: a new frontiers orbiter to study Titan's potential habitability. In: *48th Lunar and Planetary Science Conference*, p. 2306.
- Sotin, C., Lawrence, K.J., Reinhardt, B., Barnes, J.W., Brown, R.H., Hayes, A.G., Le Mouélic, S., Rodriguez, S., Soderblom, J.M., Soderblom, L.A., et al., 2012. Observations of Titan's northern lakes at 5 $\mu$ m: Implications for the organic cycle and geology. *Icarus* 221 (2), 768–786. doi:[10.1016/j.icarus.2012.08.017](https://doi.org/10.1016/j.icarus.2012.08.017).
- Stevenson, D.J., 1992. Interior of Titan. In: *Titan Symposium*. Toulouse, France, pp. 29–33.
- Stofan, E.R., Elachi, C., Lunine, J.I., Lorenz, R.D., Stiles, B., Mitchell, K.L., Ostro, S., Soderblom, L., Wood, C., Zebker, H., et al., 2007. The lakes of Titan. *Nature* 445 (7123), 61–64. doi:[10.1038/nature05438](https://doi.org/10.1038/nature05438).
- Stofan, E.R., Lunine, J.I., Lorenz, R.D., Kirk, R.L., Aharonson, O., Hayes, A.G., Lucas, A., Turtle, E.P., Wall, S.D., Wood, C.I.A., Cassini Radar Team, 2012. Shorelines of Ligeia Mare, Titan. In: *43rd Lunar and Planetary Science Conference*, p. 1556.
- Tan, S.P., Kargel, J.S., Jennings, D.E., Mastroggiuseppe, M., Adidharma, H., Marion, G.M., 2015. Titan's liquids: exotic behavior and its implications on global fluid circulation. *Icarus* 250, 64–75. doi:[10.1016/j.icarus.2014.11.029](https://doi.org/10.1016/j.icarus.2014.11.029).
- Tan, S.P., Kargel, J.S., Marion, G.M., 2013. Titan's atmosphere and surface liquid: new calculation using statistical associating fluid theory. *Icarus* 222 (1), 53–72. doi:[10.1016/j.icarus.2012.10.032](https://doi.org/10.1016/j.icarus.2012.10.032).
- Tobie, G., Lunine, J.I., Sotin, C., 2006. Episodic outgassing as the origin of atmospheric methane on Titan. *Nature* 440 (7080), 61–64. doi:[10.1038/nature04497](https://doi.org/10.1038/nature04497).
- Tokano, T., 2010. Simulation of tides in hydrocarbon lakes on saturn's moon Titan. *Ocean Dyn.* 60 (4), 803–817. doi:[10.007/s10236-010-0285-3](https://doi.org/10.007/s10236-010-0285-3).
- Tokano, T., Lorenz, R.D., 2015. Wind-driven circulation in Titan's seas. *J. Geophys. Res.-Planet* 120 (1), 20–33. doi:[10.1002/2014JE004751](https://doi.org/10.1002/2014JE004751).
- Tokano, T., Lorenz, R.D., 2016. Sun-stirred Kraken Mare: circulation in Titan's seas induced by solar heating and methane precipitation. *Icarus* 270, 67–84. doi:[10.1016/j.icarus.2015.08.033](https://doi.org/10.1016/j.icarus.2015.08.033).
- Tokano, T., Lorenz, R.D., Van Hoolst, T., 2014. Numerical simulation of tides and oceanic angular momentum of Titan's hydrocarbon seas. *Icarus* 242, 188–201. doi:[10.1016/j.icarus.2014.08.021](https://doi.org/10.1016/j.icarus.2014.08.021).
- Tseng, Q., Duchemin-Pelletier, E., Deshiere, A., Balland, M., Guillou, H., Filhol, O., Théry, M., 2012. Spatial organization of the extracellular matrix regulates cell-cell junction positioning. *Proc. Natl. Acad. Sci.* 109 (5), 1506–1511. doi:[10.1073/pnas.1106377109](https://doi.org/10.1073/pnas.1106377109).
- Turtle, E.P., Perry, J.E., Hayes, A.G., McEwen, A.S., 2011. Shoreline retreat at Titan's Ontario Lacus and Arrakis Planitia from Cassini imaging science subsystem observations. *Icarus* 212 (2), 957–959. doi:[10.1016/j.icarus.2011.02.005](https://doi.org/10.1016/j.icarus.2011.02.005).
- Tyler, R.H., 2008. Strong ocean tidal flow and heating on moons of the outer planets. *Nature* 456 (7223), 770–772. doi:[10.1038/nature07571](https://doi.org/10.1038/nature07571).
- Ventura, B., Notarnicola, C., Casarano, D., Posa, F., Hayes, A.G., Wye, L., 2012. Electromagnetic models and inversion techniques for Titan's Ontario Lacus depth estimation from Cassini RADAR data. *Icarus* 221 (2), 960–969. doi:[10.1016/j.icarus.2012.09.011](https://doi.org/10.1016/j.icarus.2012.09.011).
- Vincent, D., Karatekin, Ö., Vallaes, V., Hayes, A.G., Mastroggiuseppe, M., Notarnicola, C., Dehant, V., Deleersnijder, E., 2016. Numerical study of tides in Ontario Lacus, a hydrocarbon lake on the surface of the Saturnian moon Titan. *Ocean Dyn.* 66 (4), 461–482. doi:[10.1007/s10236-016-0926-2](https://doi.org/10.1007/s10236-016-0926-2).